© 2018. Published by The Company of Biologists Ltd | Development (2018) 145, dev163469. doi:10.1242/dev.163469

RESEARCH ARTICLE

Stratum recruits Rab8 at Golgi exit sites to regulate the basolateral sorting of Notch and Sanpodo

Karen Bellec, Isabelle Gicquel and Roland Le Borgne*

ABSTRACT

In *Drosophila*, the sensory organ precursor (SOP or pI cell) divides asymmetrically to give birth to daughter cells, the fates of which are governed by the differential activation of the Notch pathway. Proteolytic activation of Notch induced by ligand is based on the correct polarized sorting and localization of the Notch ligand Delta, the Notch receptor and its trafficking partner Sanpodo (Spdo). Here, we have identified Stratum (Strat), a presumptive guanine nucleotide exchange factor for Rab GTPases, as a regulator of Notch activation. Loss of Strat causes cell fate transformations associated with an accumulation of Notch, Delta and Spdo in the *trans*-Golgi network (TGN), and an apical accumulation of Spdo. The *strat* mutant phenotype is rescued by the catalytically active as well as the wild-type form of Rab8, suggesting a chaperone function for Strat rather than that of exchange factor. Strat is required to localize Rab8 at the TGN, and *rab8* phenocopies *strat*. We propose that Strat and Rab8 act at the exit of the Golgi apparatus to regulate the sorting and the polarized distribution of Notch, Delta and Spdo.

KEY WORDS: Asymmetric cell division, Notch signaling, Rab8, Stratum, Guanine nucleotide exchange factor, Polarized trafficking

INTRODUCTION

The Notch signaling pathway is an evolutionarily conserved cell-cell communication pathway involved in many developmental and homeostatic processes (Bray, 1998; Lai, 2004). During asymmetric cell division (ACD), one of the conserved roles of Notch signaling is to regulate cell fate decision. This process requires the interaction between the Notch receptor and Delta/Serrate/LAG-2 ligands (DSL). It leads to the proteolytic cleavage of the Notch receptor by the γ-secretase complex and to the release of its intracellular domain (NICD) in the signal-receiving cell. NICD is translocated to the nucleus where it controls target gene expression (Kopan and Ilagan, 2009; Lai, 2004). Notch receptor and DSL ligands are widely expressed throughout development, yet Notch activation is closely regulated in time and space. This spatiotemporal activation of Notch signaling is ensured in part by intracellular trafficking (Fortini and Bilder, 2009; Fürthauer and González-Gaitán, 2009; Le Borgne et al., 2005; Yamamoto et al., 2010).

The development of sensory organs (SOs) in *Drosophila melanogaster* appears to be a potent model for studying the activation of Notch signaling pathway during ACD. SOs develop from a sensory organ precursor cell (SOP) present in the single-layer epithelium of the dorsal thorax (Hartenstein and Posakony, 1989). The SOP undergoes four rounds of ACD to give rise to five cells, the fates of which are specifically governed by differential Notch activation. During ACD of SOPs, the cell fate determinants Neuralized (Neur) and Numb are unequally inherited by the anterior daughter cell (Le Borgne and Schweisguth, 2003; Rhyu et al., 1994). Neur is an E3 ubiquitin ligase that activates the ligand Delta by promoting its endocytosis (Le Borgne and Schweisguth, 2003). By contrast, Numb represses the Notch receptor in the anterior daughter cell by inhibiting the membrane localization of Spdo, a four-pass transmembrane protein required for Notch activation during ACD (Cotton et al., 2013; Couturier et al., 2013; Johnson et al., 2016; O'Connor-Giles and Skeath, 2003; Upadhyay et al., 2013). As a consequence, Notch is activated in the posterior cell that adopts the pIIa fate, whereas the anterior cell adopts the pIIb fate.

Notch activation is initiated at cytokinesis and the site of ligand-receptor interaction that leads to Notch activation has been the subject of intense research over the past decade (Benhra et al., 2011; Coumailleau et al., 2009; Couturier et al., 2012; Rajan et al., 2009; Trylinski et al., 2017). To gain new insight on this complex spatio-temporal regulation involving proper sorting of both ligand and receptor along the apico-basal axis, we screened among membrane traffic regulators (Le Bras et al., 2012). We have identified *CG7787*, which encodes the ortholog of the evolutionarily conserved mammalian suppressor of Sec4 protein (Mss4), also known as Strat in *Drosophila* (Devergne et al., 2017). The exact function and mechanism of action of Mss4 remain debated. On one hand, Mss4 has been proposed to function as a Rab GDP/GTP Exchange Factor that mediates the activation of Rab GTPases (RabGEF) by its ability to convert an inactive GDP-bound form into an active GTP-bound form (Burton et al., 1994; Itzen et al., 2006a; Zhu et al., 2001). On the other hand, Mss4 is also described as a Rab-stabilizing holdase chaperone, partly due to its weak activity as a RabGEF (Gulbranson et al., 2017; Nuoffer et al., 1997; Wixler et al., 2011). Another layer of complexity is that large scale co-immunoprecipitation assays and affinity chromatography in *Drosophila* S2 cells revealed that Mss4/Strat interacts with several Rab GTPases: Rab1, Rab3, Rab8, Rab10 and Rab35 (Gillingham et al., 2014; Guruharsha et al., 2011). The function of Mss4 and its ability to regulate the activity of these Rab proteins *in vivo* remain largely unknown.

Here, we have identified Strat as a regulator of Notch signaling within the SOP lineage. The loss of Strat causes an accumulation of Spdo/Notch and Delta at the TGN, as well as an apical accumulation of Spdo. Mutation of three conserved cryptic residues of Strat indicated that its binding to Rabs is required for its activity. Among the Rabs likely to interact with Strat, we found that Strat activity is necessary for the Golgi localization of Rab8, and that the constitutively active form, as well as the wild-type form, of Rab8 rescued *strat* phenotypes. Finally, the loss of Rab8 phenocopied the localization defects observed in *strat* mutant. We propose a model in

Univ Rennes, CNRS, IGDR (Institut de Génétique et Développement de Rennes) – UMR 6290, F-35000 Rennes, France.

*Author for correspondence (roland.leborgne@univ-rennes1.fr)

R.L., 0000-0001-6892-278X

Received 16 January 2018; Accepted 21 May 2018

Development (2018) 145, dev163469. doi:10.1242/dev.163469

which Strat recruits Rab8 at the TGN to control the exit of Notch, Delta and Spdo for subsequent correct apico-basal routing, allowing Notch activation following ACD.

RESULTS

Loss of Strat leads to *Notch* phenotypes in SOs

To validate and characterize the role of Strat in the regulation of Notch signaling, we first generated a null mutant using CRISPR/Cas9 (Fig. 1A). Briefly, we induced Cas9 cuts to remove the first exon and replaced it with a cassette containing an attP landing site using homology-directed repair (step1). *strat* homozygous animals died at late larval stage III. Lethality was also observed at the same developmental stage in *strat* overdeficiency. We then confirmed that lethality was caused by the loss of Strat as it was fully rescued by reintroducing wild-type sequence of Strat at the attP site (step 2, Fig. 1A). In order to determine the role of Strat at pupal and adult stages, we used the flippase recombinase-recombination target system (FLP-FRT) to induce mitotic clones of both wild-type and *strat* homozygous cells in a heterozygous background. Although wild-type SOs are composed of only one neuron (Fig. 1B), in clones of *strat* homozygous cells we have found that 12% of SOs contained more than one neuron and 2% of SOs were devoid of neurons corresponding, respectively, to *Notch* loss and gain of function (Fig. 1B′). Importantly, the reintroduction of the wild-type sequence of Strat rescued both *Notch* phenotypes to a large extent (data not shown, *n*=177).

To understand how loss of Strat affects SO lineage, we next imaged the ACD of SOPs and daughter cells using MARCM (Lee and Luo, 1999); this enabled us to visualize Partner of Numb (Pon) and use it as an approximation of Numb localization. In the wild-type lineage, we observed four ACDs: two planar divisions, that of the SOP and its posterior daughter cell pIIa; and two divisions orthogonal to the plane, that of the anterior pIIb daughter cell and that of pIIIb (Fig. 1C). At each cell division, Pon was unequally partitioned in one of the daughter cells: the pIIb, the glial cell, the shaft and in the neuron. In *strat* SOs, the Pon asymmetry was preserved, suggesting that cell polarity was unaffected. In agreement with this proposal, loss of Strat did not modify the localization of Bazooka (Baz, Par-3), E-cadherin and Discs large (Dlg) (Fig. S1). Although apico-basal polarity is maintained, we found two categories of defects in the orientation of cell divisions as well as in the number of divisions (Fig. 1D,D′). In the first category, we observed a series of three planar divisions: that of the SOP, which gave rise to a pIIa and a pIIa-like cell; and then that of the pIIa and pIIa-like cells that produced two sockets and two shafts (Fig. 1D, 18% of cases). This first category corresponds to a *Notch* gain-of-function phenotype. In the second category (Fig. 1D′, 29% of cases), the SOP divided within the plane of the epithelium to

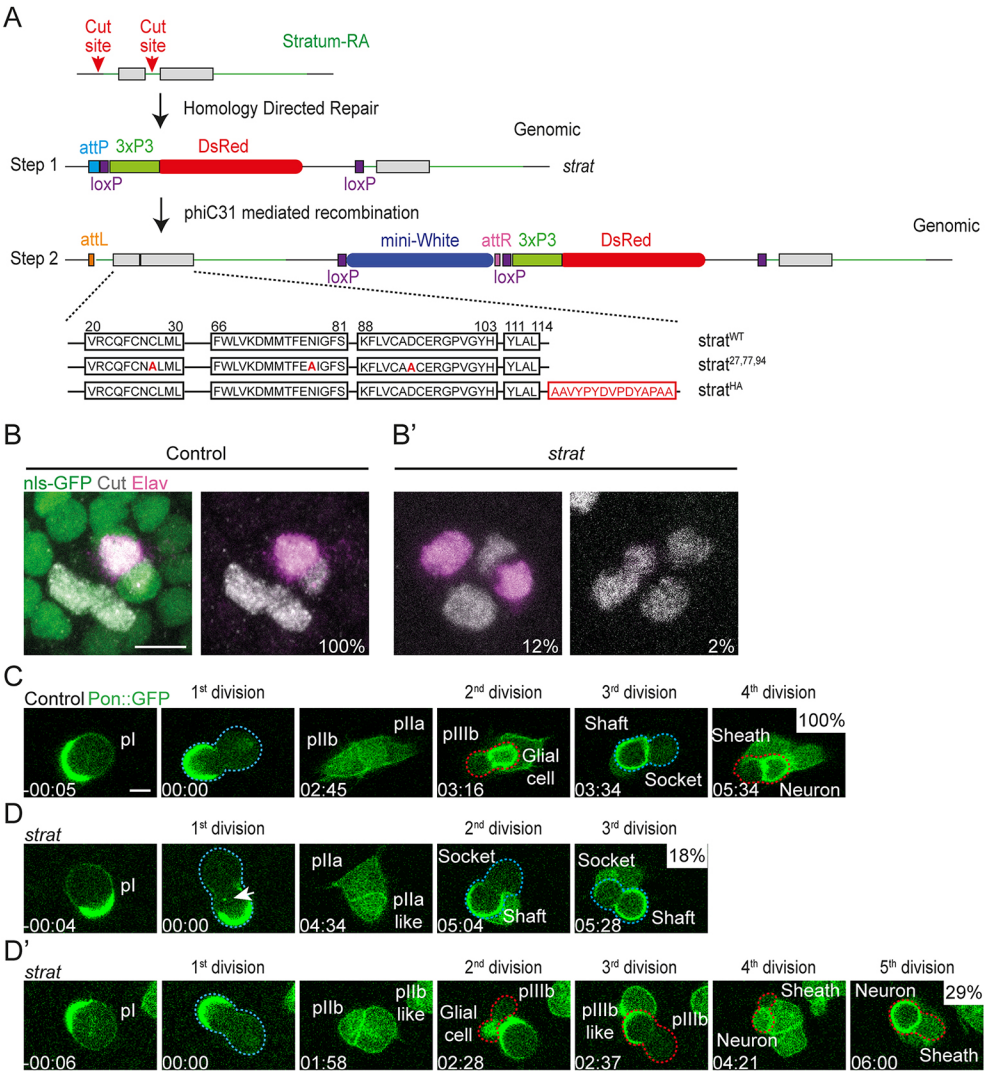

Fig. 1. Loss of Strat protein causes *Notch* loss- and gain-of-function phenotypes within the SO lineage. (A) A *strat* mutant was generated using CRISPR/Cas9 system. Cas9 cuts were induced on each side of the exon 1 (exons in gray) of *strat*. By homology-directed repair (HDR), a cassette made of an attP site (light blue), loxP sites (purple), 3xP3 promoter (green) and DsRed (red) was introduced to replace exon 1 (step 1). Wild-type sequence, mutated sequence or HA-tagged sequence of *strat*, marked with the *mini-White* cassette (dark blue), were introduced at the attP site by phiC31 integrase-mediated transgenesis (step 2) (Bischof et al., 2007). (B,B′) Projection of confocal sections of a wild-type SO (B, *n*>100) and *strat* mutant SO (B′, *n*=223) at 24 h APF. Mutant cells were identified by the absence of the nuclear marker nls-GFP. Cells of SOs were identified using Cut (anti-Cut, gray) and neurons with Elav (anti-Elav, magenta). (C-D′) Time-lapse imaging of Pon::GFP in wild-type (C, *n*=8/8) and in *strat* SO lineage (D,D′, *n*=8/34 and *n*=10/34, respectively). Dashed blue and red lines highlight planar and orthogonal cell divisions, respectively. The white arrow indicates the cytoplasmic structure positive for Pon::GFP (D, *n*=4/34). Time is in hour:minute and the time 00:00 corresponds to SOP anaphase onset. Scale bars: 5 µm.

Development (2018) 145, dev163469. doi:10.1242/dev.163469

generate a pIIb and pIIb-like cells that in turn divided perpendicular to the plane of the epithelium. In this category, corresponding to *Notch* loss of function, we observed up to seven ACDs producing an excess of neurons. We conclude that loss of Strat causes either *Notch* loss- or *Notch* gain-of-function phenotypes by affecting cell fate acquisition during the SOP division. For the rest of this study, we therefore concentrated on SOP division.

Notch signaling defects observed in the absence of Strat depend on the activity of cell fate determinants

Surprisingly, in MARCM clones, the rates of cell fate transformations were largely increased compared with simple *strat* clones (Fig. 1B′ versus Fig. 1D,D′). Because, in MARCM clones, Pon was overexpressed under the control of the SOP-specific driver $neur^{P72}$-GAL4, a hypomorphic allele of *neur*, we hypothesized that the increased phenotypes could be caused either by the excess of Pon or the loss of one copy of *neur*, or both. To test these hypotheses, we first removed one copy of *neur* in *strat* and found that the *Notch* gain-of-function phenotype was increased at the expense of the loss-of-function phenotype (Fig. 2A), explaining in part the modification of *strat* phenotypes observed in MARCM clones. Second, to avoid the side effect caused by Pon overexpression (Perdigoto et al., 2008), we added one copy of *numb*, using a functional bacterial artificial chromosome (BAC) rescue NumbGFP construct (Couturier et al., 2013). We found that three copies of *numb* in *strat* mutant cells led to an increase of the *Notch* gain-of-function phenotype (Fig. 2A). As in control SOP, Neur, Numb and NumbGFP localized asymmetrically in the *strat* mutant, suggesting that *strat* phenotypes and the increased *Notch* phenotype observed when changing the copy numbers of *neur* and *numb* was unlikely due to a defect in the unequal partitioning of these cell fate determinants (Fig. 2B-C′ and Fig. S2A,A′). However, although Numb remained restricted to the anterior cortex at prometaphase in most *strat* cells (Fig. 2C,C′), in a few cases

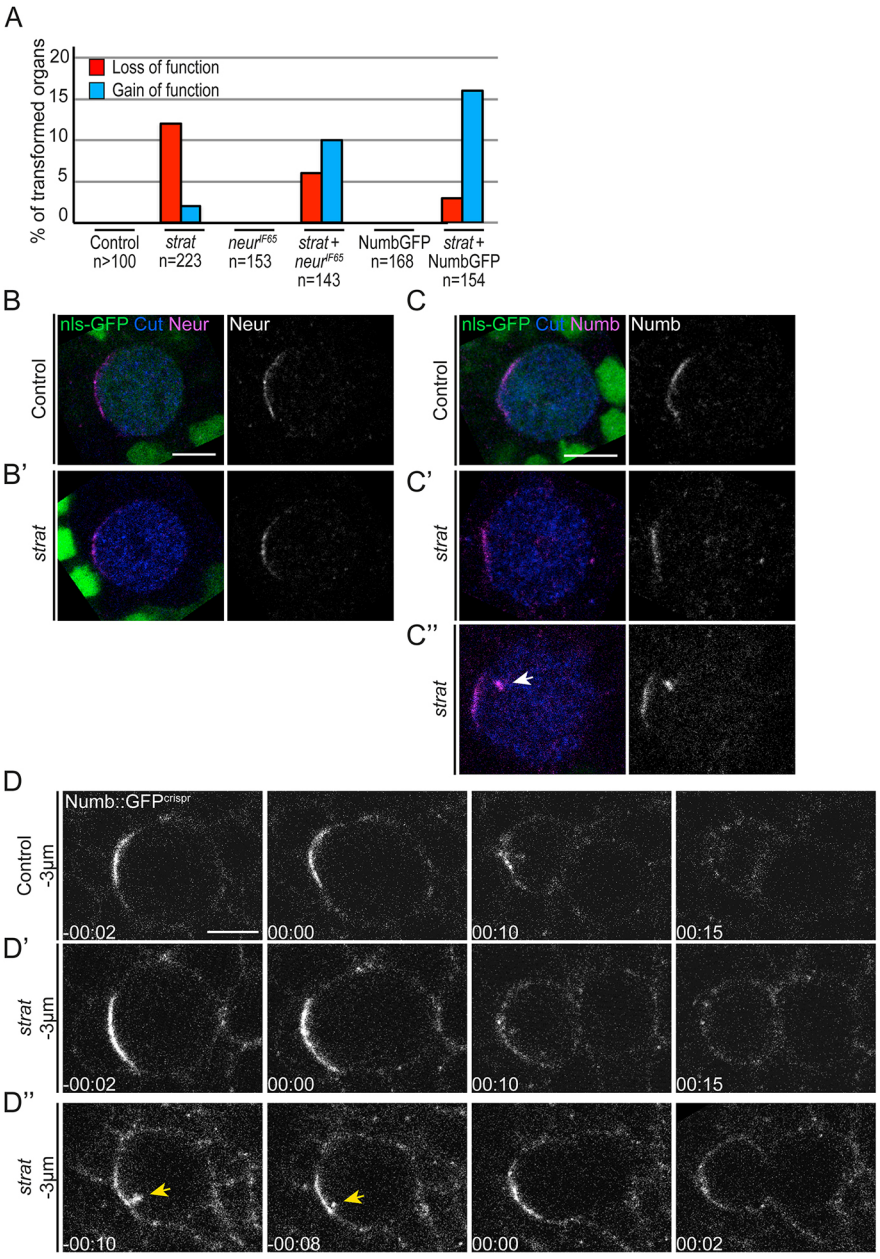

Fig. 2. *strat* interacts with *neur* and *numb* but does not control their unequal partitioning. (A) Histogram of the percentage of transformed organs in wild-type SOs, *strat* SOs, SOs heterozygous for *neur*, *strat* SOs heterozygous for *neur*, SOs expressing NumbGFP and *strat* SOs expressing NumbGFP. The *Notch* loss-of-function phenotype and *Notch* gain-of-function phenotype are represented in red and blue, respectively. (B-C″) Localization of Neur (anti-Neur, magenta) and Numb (anti-Numb, magenta) in wild-type (B, *n*=17 and C, *n*=26) and *strat* (B′, *n*=10; C′, *n*=15/18 and C″, *n*=3/18) SOPs. SOPs are stained using anti-Cut (blue). The white arrow indicates the cytoplasmic structure positive for Numb. C′ and C″ correspond to two different categories of *strat* mutant phenotype (18 *strat* mutant SOs were analyzed, among which 15 fell into the category shown in C′ and three fell into the category shown in C″). (D-D″) Time-lapse imaging of Numb::GFP^{crispr} in wild-type SOPs (D, *n*=5) and *strat* SOPs (D′, *n*=5/6 and D″, *n*=1/6). The yellow arrows indicate the cytoplasmic structure labeled with Numb::GFP^{crispr}. Time is in hour:minute and the time 00:00 corresponds to the SOP anaphase onset. Scale bars: 5 µm.

Development (2018) 145, dev163469. doi:10.1242/dev.163469

Numb was also detected on punctate intracellular structures (Fig. 2C″, 17% of cases). Live imaging of Numb::GFP^{crispr}, a GFP-tagged version of Numb generated by CRISPR/Cas9, further confirmed that Numb was properly asymmetrically localized in prometaphase to be unequally segregated in the pIIb cell at telophase in the majority of *strat* mutant SOs (Fig. 2D,D′). We also found a case where Numb::GFP^{crispr} localized on a cytoplasmic punctate structure in prometaphase (Fig. 2D″, 17% of cases). Nonetheless, ultimately Numb::GFP^{crispr} was unequally segregated in the anterior cell. Of note, Pon::GFP and NumbGFP also localized in punctate structures in MARCM experiments, and this correlated with a *Notch* gain-of-function phenotype (Fig. 1D, 18% of cases and Fig. S2A″, 25% of cases). Thus, Strat could prevent Numb and Pon from localizing on punctate structures during mitosis. Whether this change in distribution directly caused the *Notch* gain of function is currently unknown. However, we do not favor the idea that the punctate structure may cause a reduction in amount of Numb available to inhibit Notch, i.e. that Numb would become rate limiting upon loss of Strat. Indeed, if this were the case, the addition of one extra copy of *numb* should have suppressed, at least in part, the *Notch* gain-of-function phenotype. By contrast, we observed the opposite phenotype, suggesting that the *Notch* phenotype caused by the loss of Strat is due to its downstream effectors (Fig. 2A).

Strat regulates Spdo localization

As Numb regulates Spdo localization (Cotton et al., 2013; Couturier et al., 2013; Hutterer and Knoblich, 2005; Langevin et al., 2005), the genetic interaction observed between *numb* and *strat* led us to study the localization of Spdo in *strat* SOs (Fig. 3A). As expected (Cotton et al., 2013; Couturier et al., 2013; Hutterer and Knoblich, 2005; Langevin et al., 2005), at the two-cell stage, Spdo was localized in endosomal compartments in the anterior pIIb cell, and at the basolateral plasma membrane of the posterior pIIa cell (Fig. 3B and Movie 1). A faint Spdo signal was also detected apically. By contrast, Spdo was enriched at the apical pole as well as in intracellular compartments in *strat* SOP daughters (Fig. 3B′,C and Movie 2). Similar mislocalizations of Spdo were also observed in SOP during interphase, indicating that Strat controls Spdo localization prior to, and following, the division of SOP (Fig. S3A,A′).

To gain insight on the role of Strat in Spdo trafficking, we next live imaged SpdoiGFP BAC rescue construct (Fig. 3D,D′) (Couturier et al., 2013). In wild-type SOs, SpdoiGFP was detected at the apical cortex of interphase SOP and enriched at the apical interface between the SOP daughters (Fig. 3D). At the level of nuclei, SpdoiGFP was localized into cytoplasmic structures in interphase SOPs, and in the anterior pIIb cell at the two-cell stage as reported previously (Couturier et al., 2013), Fig. 3D). In *strat*, we first observed that a supplemental copy of *spdo* strongly enhanced the *Notch* gain-of-function phenotype, demonstrating that *strat* and *spdo* genetically interact (Fig. 3E). Second, as observed for endogenous Spdo on fixed specimen (Fig. 3B′), loss of Strat also led to an apical accumulation of SpdoiGFP in interphase SOPs and at the two-cell stage (Fig. 3D′). However, and contrary to the data obtained using the anti-Spdo antibody, SpdoiGFP was not accumulated in intracellular compartments in *strat* mutant cells. These surprising results prompted us to compare the localization of the fluorescent GFP signal of SpdoiGFP with that of the anti-GFP antibody (Fig. 3F,F′). It is striking that only a subpopulation of intracellular compartments detected with the anti-GFP was GFP-fluorescent in *strat* (Fig. 3F′). A similar observation was made with the Notch::GFP^{crispr} that we have generated (Fig. S3B,B′). Fluorescent signal of SpdoiGFP and Notch::GFP^{crispr} might not be detected in some intracellular compartments because either GFP was not yet folded or, alternatively, these compartments had an acidic pH quenching the GFP signal, as reported previously (Couturier et al., 2014). This raised the question of the identity of these compartments. We did not observe change in colocalization between Spdo- and Rab11-positive recycling endosomes nor the early endosomal marker hepatocyte growth factor-regulated tyrosine kinase substrate (HRS) in *strat* mutant cells (Fig. S4B,B′,C,C′). Instead, we found that the anti-GFP-positive and SpdoiGFP-negative compartments were closely juxtaposed to the *cis*-Golgi compartment, identified by the Golgi matrix protein of 130 kDa (GM130; Fig. 3F′; Kondylis et al., 2001). Upon loss of Strat, endogenous Spdo was also closely juxtaposed to GM130 (Fig. 4A,A′,C) and colocalized with the TGN marker Syntaxin16 (Syx16; Fig. 4B,B′,C; Xu et al., 2002) as well as with the clathrin adaptor protein complex-1 (AP-1; Fig. S4A,A′). Altogether, these results demonstrate that the loss of Strat causes the accumulation of Spdo in the TGN and at the apical pole of SOPs and daughter cells. These accumulations of Spdo were not modified by the extra copy of *numb* (Fig. S4D,D′), showing that the defective localizations of Spdo were effectively associated with *Notch* phenotypes. These data raise the question of the localization of core Notch components in *strat* SOs.

In *strat*, Notch and Delta accumulate with Spdo at the TGN

As Spdo and Notch interact and traffic together, and Spdo is required for ligand-dependent Notch activation (Couturier et al., 2013; Upadhyay et al., 2013), we then studied the localization of Notch and its ligand Delta in *strat*. We found that Notch and Delta were accumulated together with Spdo in the TGN (Fig. 4D-F; Fig. S4E,F). To investigate whether it was the newly synthesized Spdo and Delta that were accumulated in TGN rather than pools of Delta and Spdo that were internalized and recycled via the TGN, we performed pulse-chase internalization assays as described previously (Benhra et al., 2011; Cotton et al., 2013). Briefly, Delta endocytosis was monitored using the anti-DECD antibody whereas that of Spdo was performed using the SpdoL2::mChFP transgene, which was recognized by an anti-RFP antibody. Cells were first pulsed-labeled using anti-DECD and anti-RFP antibodies at 4°C to label the pools of Delta and SpodL2 present at the plasma membrane, and then chased at 25°C to allow endocytosis for 15 min (Fig. 5A). This qualitative assay was used to determine the ability of a given protein to be internalized and reach a defined intracellular compartment. The presence of intracellular structures containing both anti-RFP and anti-DECD demonstrated first that SpdoL2 and Delta are efficiently internalized in both control and *strat* SOs (Fig. 5B,B′). Both in control and *strat* SOs the intracellular compartments containing Spdo and internalized Delta were negative for GM130 (Fig. 5C,C′). These data indicate that Strat does not regulate endocytosis. In addition, the accumulation of Spdo and Delta in the TGN is unlikely due to their recycling from the plasma membrane to the Golgi apparatus.

However, this assay only tests for internalization from the basolateral membrane. Indeed, extracellularly added antibodies do not have access to the apical plasma membrane because of the impermeable apical cuticle and the presence of cellular junctions that physically separate the apical from the basolateral plasma membrane. Thus, as an approximation for apical endocytosis, we tested the dynamics of Spdo that accumulates apically upon loss of Strat by using a Spdo::Dendra2 transgene: a green to red photoconvertible probe (Fig. S5). We reasoned that, if Strat controls the apical endocytosis, its loss could lead to clustering of Spdo in forming endocytic structures unable to bud from the plasma membrane. In that case, a photoconverted pool of Spdo in a region of interest (ROI) (Fig. S5A) would not diffuse laterally (Fig. S5A, top panels).

Development (2018) 145, dev163469. doi:10.1242/dev.163469

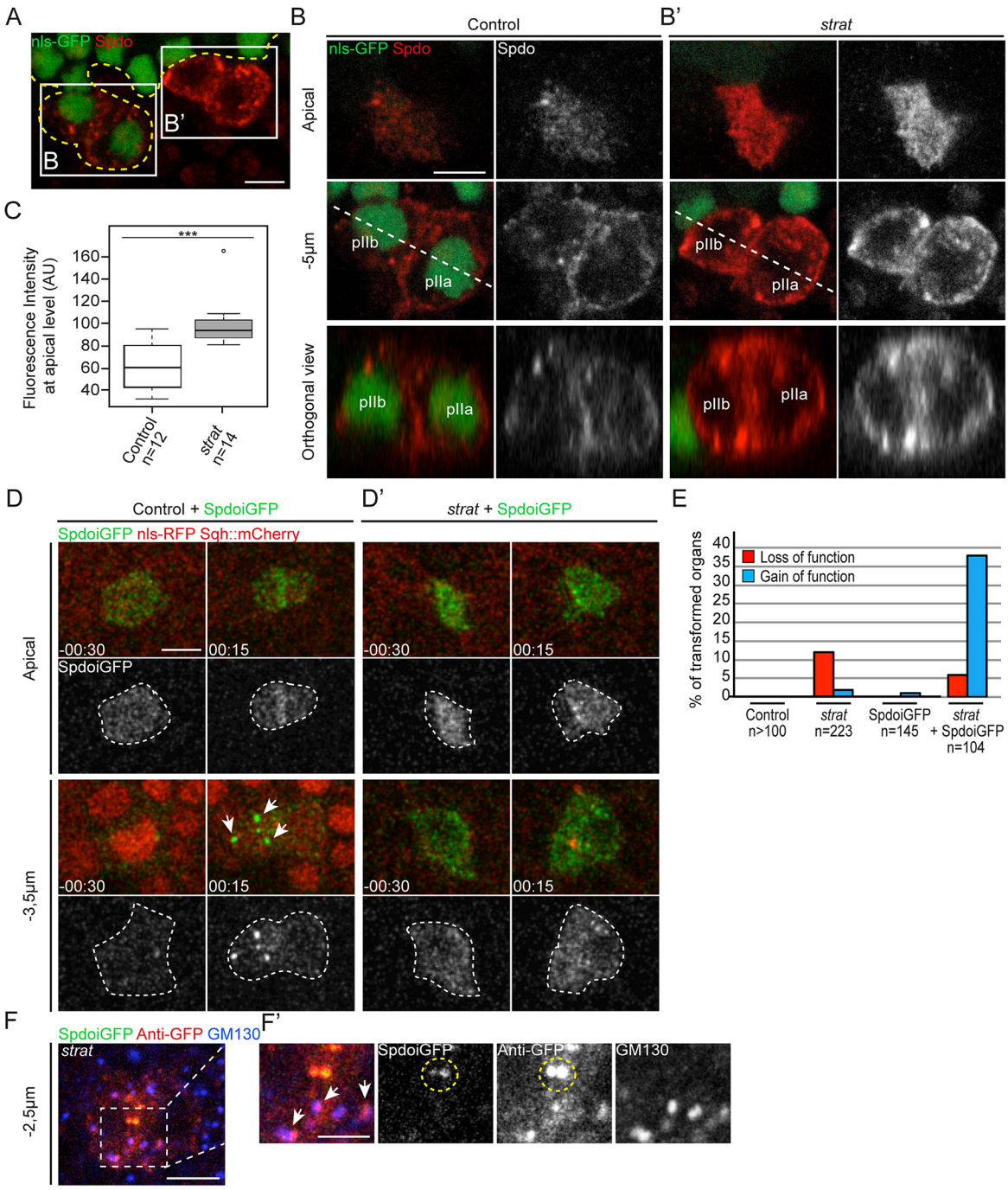

Fig. 3. Spdo localization is regulated by Strat. (A) Localization of Spdo (anti-Spdo, red). Wild-type and *strat* cells are separated by the dashed yellow line. Wild-type and *strat* SOP daughter cells are framed by a white rectangle and enlarged in B,B′. (B,B′) Localization of Spdo in wild-type (B) and *strat* SOP daughter cells (B′). Dashed white lines indicate the position of orthogonal sections. (C) Box plots showing the fluorescence signal intensity of Spdo at the apical level in wild-type and *strat* SO (***P-value<0.001). The line is the median and the box represents the values included between the 25th and 75th percentiles. (D,D′) Time-lapse imaging of SpdoiGFP and Myosin (Sqh::mCherry) in wild-type (D, n=5) and *strat* (D′, n=6) SOPs. Dashed white lines highlight SOP daughter cells. White arrows indicate intracellular compartments positive for SpdoiGFP. Time is in hour:minute and the time 00:00 corresponds to the SOP anaphase onset. (E) Histogram of the percentage of transformed organs in wild-type SOs, *strat* SOs, SOs expressing SpdoiGFP and *strat* SOs expressing SpdoiGFP. *Notch* loss-of-function phenotype and *Notch* gain-of-function phenotype are represented in red and blue, respectively. (F) Localization of SpdoiGFP (SpdoiGFP, green and anti-GFP, red) and the *cis*-Golgi marker (anti-GM130, blue) in *strat* SOP daughter cells. The dashed white rectangle delineates the high magnification (electronic zoom) shown in F′. Dashed yellow circles surround intracellular compartments positive for both SpdoiGFP and anti-GFP. White arrows indicate intracellular compartments positive for both anti-GFP and anti-GM130. Scale bars: 5 µm (3 µm for the high magnification).

Conversely, if Strat does not control apical endocytosis, Spdo is anticipated to freely diffuse at the apical pole. In this case, the photoconverted pool of Spdo would be expected to be in rapid exchange and to mix with the non-photoconverted Spdo (Fig. S5A, bottom panels). Prior to photoconversion, as shown for endogenous Spdo, Spdo::Dendra2 is accumulated at the apical pole of *strat* SOs (Fig. S5B). We observed that following photoconversion, the photoconverted Spdo::Dendra2 diffused

Development (2018) 145, dev163469. doi:10.1242/dev.163469

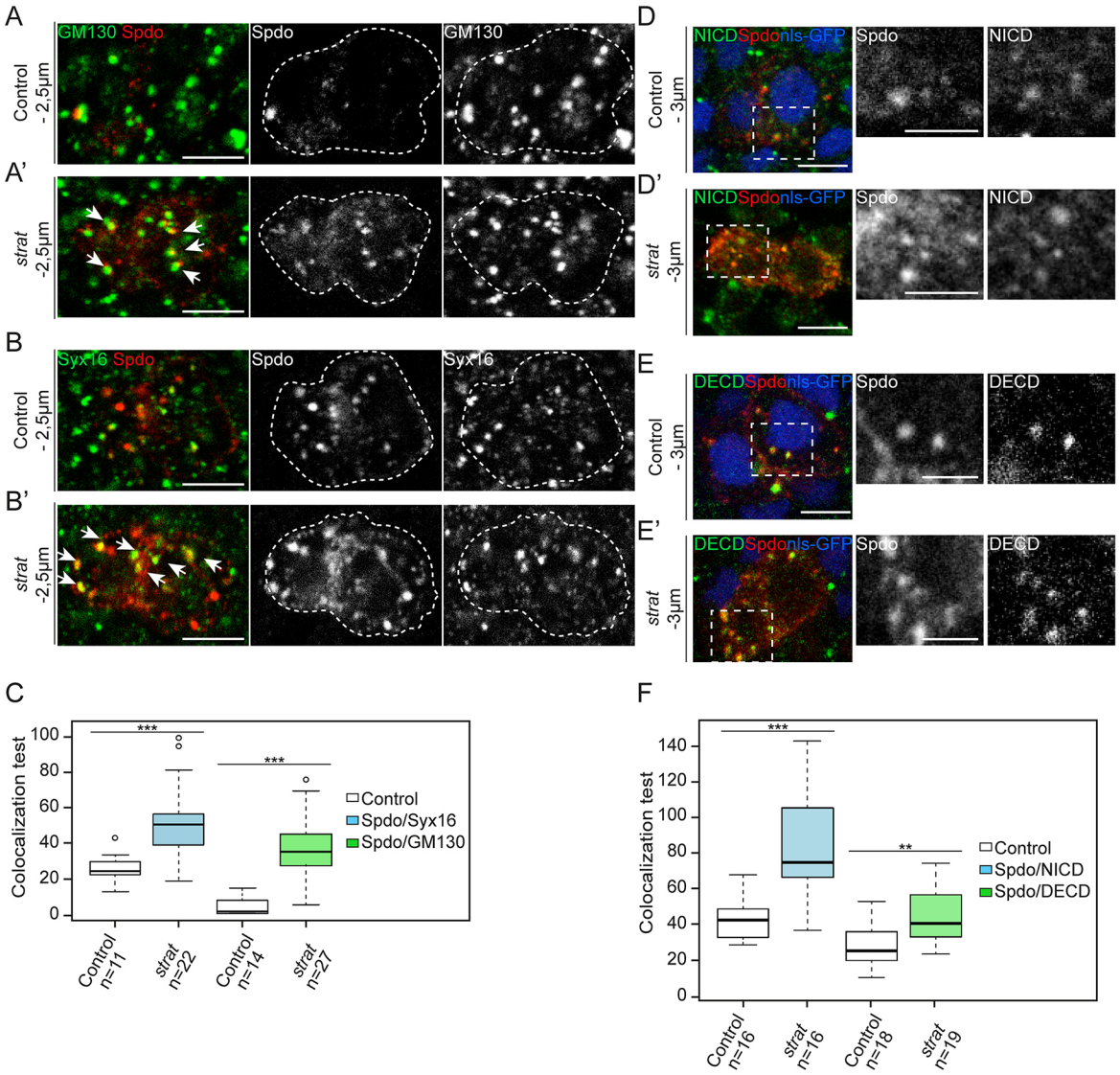

Fig. 4. Loss of Strat causes the accumulation of Notch, Spdo and Delta at the exit of the Golgi apparatus. (A,A′) Localization of Spdo (anti-Spdo, red) and the *cis*-Golgi marker GM130 (anti-GM130, green) in wild-type (A) and *strat* SOP daughter cells (A′). The dashed white line highlights SOP daughter cells. White arrows indicate the enrichment of Spdo in intracellular compartments positive for GM130. (B,B′) Localization of Spdo (anti-Spdo, red) and the *trans*-Golgi marker Syx16 (anti-Syx16, green) in wild-type (B) and *strat* (B′) SOP daughter cells. The dashed white line highlights SOP daughter cells. White arrows indicate the enrichment of Spdo in intracellular compartments positive for Syx16. (C) Box plots showing the colocalization between Spdo and Golgi markers in wild-type and *strat* SOP daughter cells (***P<0.001). The line is the median and the box represents the values included between the 25th and 75th percentiles. (D,D′) Localization of Spdo (anti-Spdo, red) and Notch (anti-NICD, green) in wild-type (D) and *strat* (D′) SOP daughter cells. Dashed white rectangles delineate the high magnification (electronic zoom) shown in the right panels. (E,E′) Localization of Spdo (anti-Spdo, red) and Delta [anti-Delta extracellular domain (DECD), green] in wild-type (E) and *strat* (E′) SOP daughter cells. Dashed white rectangles delineate the high magnification (electronic zoom) shown in the right panels. Scale bars: 5 µm (3 µm for electronic zooms). (F) Box plots showing the colocalization between Spdo and Notch and between Spdo and Delta in wild-type and *strat* SOP daughter cells (***P<0.001 and **P<0.01). The line is the median and the box represents the values included between the 25th and 75th percentiles.

outside the ROI within the apical pole in a second time scale (Fig. S5B,C). Keeping in mind that, because our photoconversion assay did not directly monitor endocytosis, we cannot firmly exclude the possibility that impaired apical endocytosis could, in part, be responsible for apical accumulation of Spdo. Collectively our data suggest that Strat is primarily required for the exit of newly synthesized Spdo/Notch and Delta from the TGN.

Strat controls the localization of Rab8 at the TGN

To obtain some insight on how Strat could regulate TGN exit of Spdo/Notch and Delta, we first localized Strat. Having failed to raise anti-Strat antibody, we reintroduced a HA tag version of *strat* at the locus (Fig. 1A) that, in contrast to the wild-type version, failed to rescue the lethality and *Notch* phenotypes. This was likely due to the expression level of the tagged version, as overexpressing the functional Strat::HA described by Devergne et al. (2017) fully rescued the *Notch* phenotypes (data not shown, n=115). Strat::HA was found to localize in close proximity to GM130 and to colocalize with Syx16, indicating that Strat localized at the TGN (Fig. 6A).

Strat was initially proposed to function either as a GEF or as a chaperone to control the activity of one or several Rab GTPases (Burton et al., 1994; Itzen et al., 2006a; Zhu et al., 2001). In agreement with these proposals, we found that a version of Strat mutated on conserved residues (C27A, N77A and D94A), which is

Development (2018) 145, dev163469. doi:10.1242/dev.163469

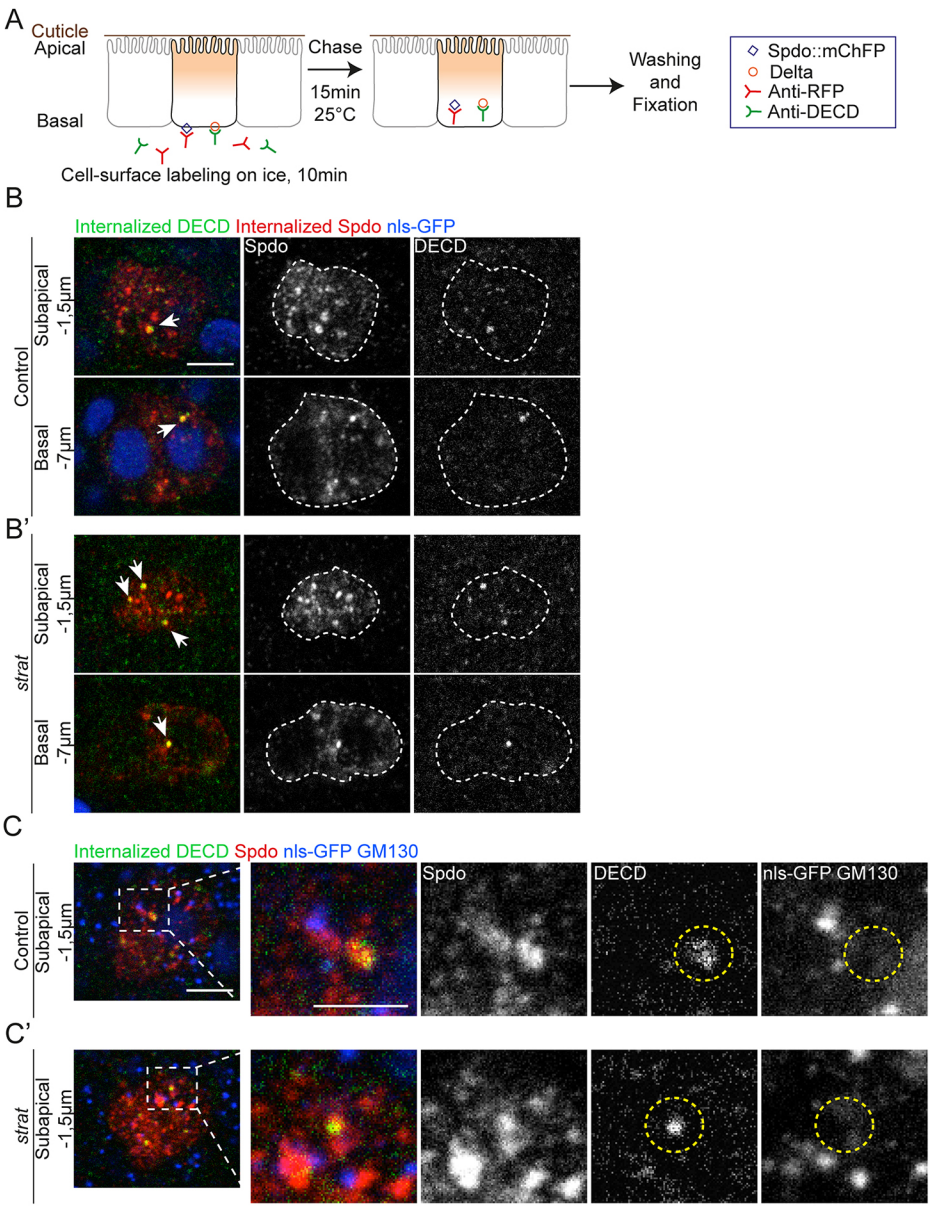

Fig. 5. Internalization of Spdo and Delta takes place in the absence of Strat. (A) Schematic representation of the cell-surface labeling and antibody-uptake experiments. The UAS-SpdoL2::mChFP construct is represented by a dark-blue square, Delta is represented by an orange circle, anti-RFP antibodies are represented in red and anti-DECD antibodies in green. (B,B′) A 10 min pulse of anti-RFP (Spdo, red) and anti-Delta (green) at 4°C, followed by a 15 min chase internalization in wild-type (B) and *strat* (B′) SOP daughter cells. The dashed white line highlights SOP daughter cells. White arrows indicate intracellular compartments positive for both Spdo and Delta. (C,C′) A 10 min pulse of anti-Delta (green) followed by a 15 min chase internalization in wild-type (C) and *strat* (C′) at the SOP daughter cells. Following fixation, nota were stained to visualize the *cis*-Golgi marker GM130 (anti-GM130, blue) and Spdo (anti-Spdo, red). Dashed white rectangles delineate high magnification (electronic zooms) shown in the right panels. Yellow circles surround intracellular compartments positive for Delta. Scale bars: 5 µm (3 µm for electronic zooms).

required for its interaction with Rab, was unable to rescue the lethality caused by loss of Strat (Fig. 1A) (Itzen et al., 2006a; Zhu et al., 2001). Co-affinity purification followed by mass spectrometry and affinity chromatography assays revealed that Strat can physically interact with Rab1, Rab3, Rab8, Rab10 and Rab35 (Devergne et al., 2017; Gillingham et al., 2014; Guruharsha et al., 2011). To decipher which Rab(s) among these could be regulated by Strat *in vivo*, we analyzed their respective localization in *strat* cells using antibodies and/or endogenous YFP-tagged Rab proteins (Dunst et al., 2015). We found that Rab3 was undetectable in the dorsal thorax, and that the localization of Rab1 and Rab35 was not affected by the loss of Strat (Fig. S6A,B). This contrasted with Rab8 and, to a lesser extent, Rab10, the localization of which was severely affected by loss of Strat (Fig. 6B,B′, Fig. S6C,C′,D). In *strat* cells, the intensity of Rab8^{EYFP} (Dunst et al., 2015), as well as that of endogenous untagged Rab8 (Mavor et al., 2016), were strongly reduced (Fig. 6B,B′ and Fig. S6C,C′). We found that Rab8 colocalized with GM130 and in part with Spdo in wild-type cells (Fig. 6C-D″), a localization that was lost in *strat* SOs (Fig. 6C″,D′,D″). To test whether the reduction in Rab8 straining in *strat* clones could be due to degradation as proposed in mammalian cells (Gulbranson et al., 2017), we performed western blot analyses. Because such an experiment was impossible on mosaic tissues, we switched to brain extracts of *strat* homozygote larvae, prior to the death of the animal, after making sure that Rab8 localization was also dependent on Strat in this tissue (Fig. 6E,E′). We found that the expression level and/or stability of Rab8 was unmodified upon loss of Strat, indicating that Strat regulates the TGN localization of Rab8, rather than its stability (Fig. 6F and Fig. S6E).

We next reasoned that if Strat activates Rab8 by promoting its loading in GTP, the *strat* phenotype was expected to be rescued by the expression of the constitutively active, GTP-bound form of Rab8. We found that overexpression of Rab8Q67L, but not that of Rab10Q68L or Rab35Q67L, rescued the *Notch* phenotypes (Fig. 6G and data not shown). Nonetheless, *Notch* phenotypes, as well as mislocalization of Spdo and Notch, were also rescued by the overexpression of the wild-type form of Rab8 in *strat* mutant cells (Fig. 6G; Fig. S6F,F′,G,G′,H). Although these data dot not unambiguously determine whether Strat acts as a GEF or a chaperone (see Discussion), they indicate that Strat acts through

Development (2018) 145, dev163469. doi:10.1242/dev.163469

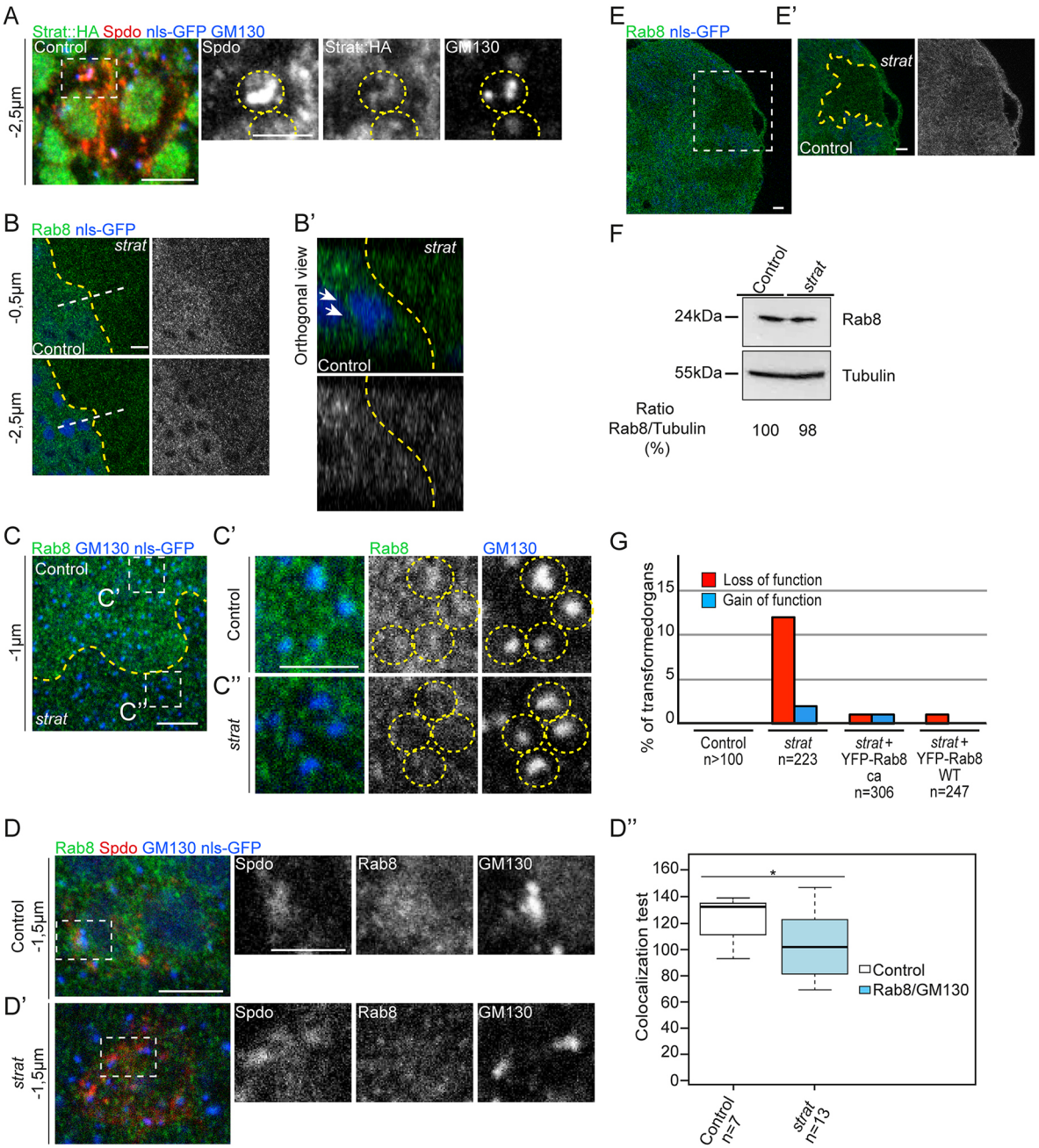

Fig. 6. Strat controls the localization and activates GTPase activity of Rab8. (A) Localization of Spdo (anti-Spdo, red), Strat::HA (anti-HA, green) and GM130 (anti-GM130, blue) in wild-type two-cell stage SOs. Dashed white rectangles delineate high magnifications (electronic zoom) shown in the right panels. The nuclear HA staining is specific as it is not detected outside the GAL4 expression domain (data not shown). Dashed yellow circles surround intracellular compartments positive for Strat::HA, Spdo and GM130. (B,B′) Localization of Rab8 (anti-Rab8, green) in pupal nota. Wild-type and *strat* cells are separated by a dashed yellow line. (B′) Orthogonal sections along the white dashed line depicted in B. White arrows show examples of compartments positive for Rab8. (C-C″) Localization of Rab8 (anti-Rab8, green) and GM130 (anti-GM130, blue) in nota of pupae. Wild-type and *strat* cells are separated by a dashed yellow line. Dashed white rectangles delineate high magnifications (electronic zoom) shown in C′,C″. Dashed yellow circles surround intracellular compartments positive for Rab8 and GM130 in wild-type and only positive for GM130 in *strat*. (D,D′) Localization of Spdo (anti-Spdo, red), Rab8 (anti-Rab8, green) and GM130 (anti-GM130, blue) in *strat* SOP daughter cells. Dashed white rectangles delineate high magnifications (electronic zoom) shown in the right panels. (D″) Box plots showing the colocalization between Rab8 and GM130 in wild-type and *strat* SOP daughter cells (*P<0.05). The line is the median and the box represents the values included between the 25th and 75th percentiles. (E,E′) Localization of Rab8 (anti-Rab8, green) in brains of larvae. Wild-type and *strat* cells are separated by a dashed yellow line. The dashed white rectangle delineates the high magnification shown in E′. Scale bars: 5 µm (3 µm for high magnifications and electronic zooms). (F) Western blot analysis showing Rab8 level in brains of wild-type and *strat* from larval stage 3 (n=2). Tubulin was used as a loading control. (G) Histogram of percentage of transformed organs in wild-type SO, in *strat* SO, in *strat* SO expressing the constitutively active form of Rab8 and the wild-type form of Rab8. *Notch* loss-of-function phenotype and *Notch* gain-of-function phenotype are represented in red and blue, respectively.

Rab8 at the TGN to allow the sorting of Spdo, Notch and Delta. This proposal was further supported by the observation that, as seen in *strat* mutant, Spdo was enriched at the apical pole as well as in intracellular compartments positive for GM130 in SOs mutant for a null allele of Rab8: $rab8^{U1}$ (Fig. 7A-B). We propose that Strat recruits Rab8 at the TGN to control the exit of Spdo/Notch and

Development (2018) 145, dev163469. doi:10.1242/dev.163469

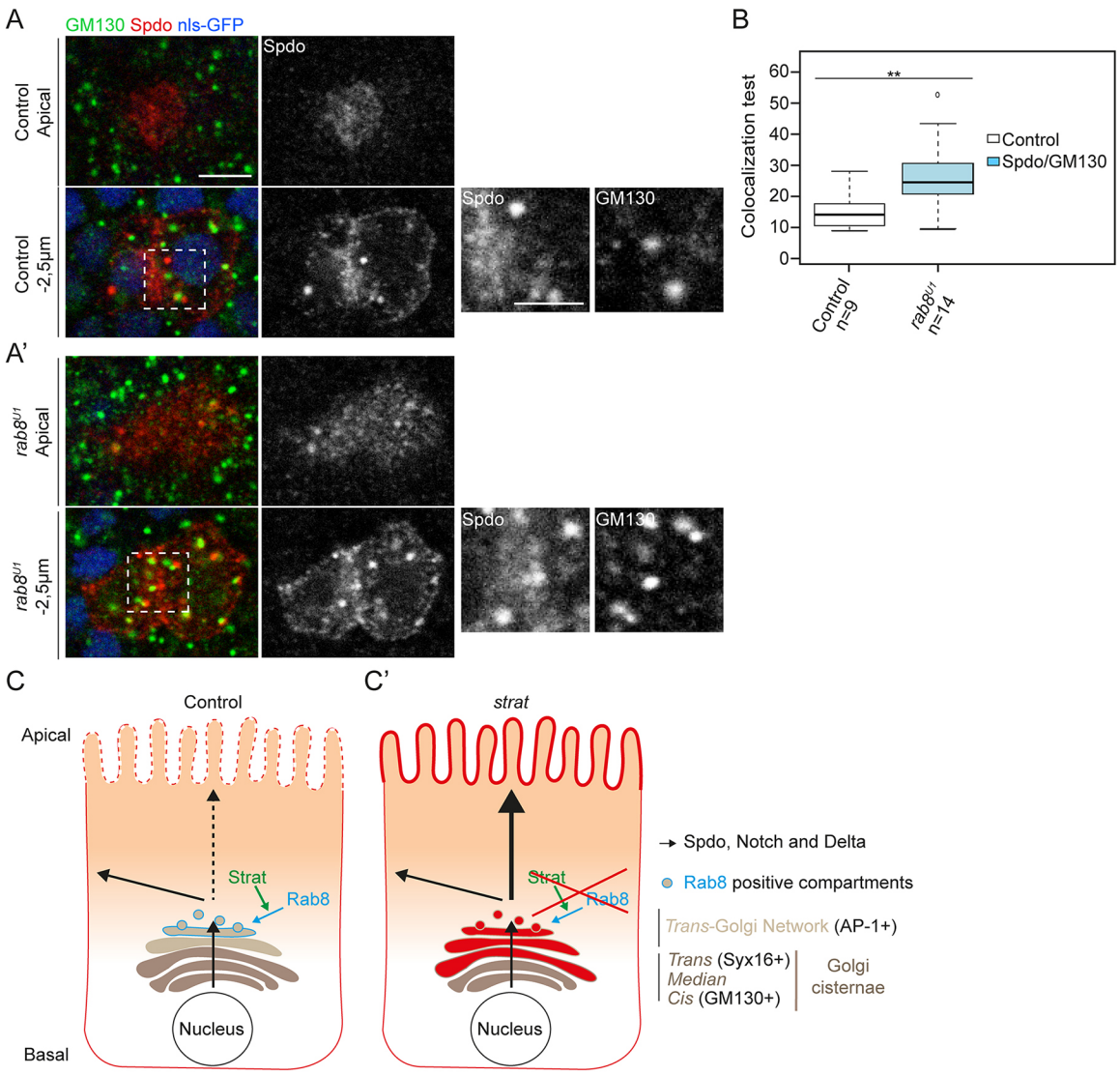

Fig. 7. Model of Strat function to regulate the Golgi localization of Rab8 to control the basolateral sorting of Spdo, Notch and Delta. (A,A′) Localization of Spdo (anti-Spdo, red) and GM130 (anti-GM130, green) in wild-type (A) and *rab8*^{U1} (A′) at the two-cell stage. Dashed white rectangles delineate high magnifications (electronic zoom) shown in the right panels. Scale bars: 5 µm (3 µm for high magnifications and electronic zooms). (B) Box plots showing the colocalization between Spdo and GM130 in wild-type and *strat* SOP daughter cells (**P<0.01). The line is the median and the box represents the values included between the 25th and 75th percentiles. (C,C′) Model of Strat/Rab8 function in the regulation of Spdo, Notch and Delta trafficking in wild-type (C) and *strat* (C′) SOs. Spdo, Notch and Delta trafficking is represented with black arrows; Rab8 is depicted in blue; the enrichment of Spdo, Notch and Golgi in intracellular compartments and the apical enrichment of Spdo are depicted in red; cisternae are represented in dark brown and the TGN is represented in light brown.

Delta from this compartment for subsequent correct apicobasal sorting (Fig. 7C,C′).

DISCUSSION

Here, we report that Strat is a novel regulator of Notch activation following SOP division. Strat is unlikely to be a general membrane trafficking controller, as the apico-basal polarity of epithelial cells and the asymmetric division of SOPs in terms of the length of mitosis, cell size asymmetry and unequal partitioning of cell fate determinants, are unaffected by loss of Strat. Strat is instead involved in specific intracellular sorting and transport because the loss of Strat protein leads to the accumulation of Notch, Delta and Spdo at the TGN, and to the improper apical accumulation of Spdo (Fig. 7C′). We found that Strat is needed for the recruitment of Rab8 at the TGN, that loss of Strat was rescued by the overexpression of a catalytic active or a wild-type version of Rab8, and that loss of Rab8 recapitulated Spdo mislocalization defects observed in *strat*. We propose a model according to which Strat localizes Rab8 at the TGN to ensure the sorting and exit of cargoes for subsequent basolateral targeting, thus ensuring proper spatio-temporal activation of the Notch pathway following SOP division (Fig. 7C).

Involvement of Strat for Notch activation following ACD

In *strat*, the large majority of SOs developed properly (86% of SOs), suggesting that Notch signaling occurred correctly regardless of the highly penetrant localization defects of Notch, Delta and Spdo (100% of SOs). Indeed, despite these changes in location, the steady state localization of Notch at the plasma membrane was unchanged. Similarly, we did not detect changes in the plasma membrane localization of Delta on fixed specimens. As the novel membrane interface formed between SOP daughter cells at cytokinesis is the major activation site of Notch proteolytic

Development (2018) 145, dev163469. doi:10.1242/dev.163469

activation (Couturier et al., 2012; Trylinski et al., 2017), these data could explain why SO development occurs normally in most cases upon loss of Strat. The weak *Notch* gain and loss-of-function phenotypes could be attributed to slight modification of cell surface levels and/or loss of asymmetries of Notch/Delta/Spdo at the pIIa/pIIb cell interface that could be difficult to quantitatively detect with our live-imaging and immunostaining assays.

However, one additional copy of *spdo* in *strat* cells strongly increased the *Notch* gain-of-function phenotype suggesting that Spdo was somehow rate limiting in the expressivity of the *Notch* phenotype induced by the loss of Strat. In a control situation, Numb prevents the recycling of Spdo to the plasma membrane by promoting the localization of Spdo and Notch in endosomes in the pIIb cell (Cotton et al., 2013; Couturier et al., 2013; Hutterer and Knoblich, 2005; Langevin et al., 2005; Tong et al., 2010). Interestingly, in *strat*, SpdoiGFP was no longer detected in these endosomal compartments. We report that this was not due to a defect of Numb unequal partitioning nor to a defect in Spdo endocytosis. It was also unlikely that Strat reduced Numb activity because the addition of one copy of *numb* worsened the *Notch* gain-of-function phenotype of *strat*. However, this result was puzzling as it was expected that an additional copy of this negative Notch regulator would reduce the *Notch* gain-of-function phenotype induced by the loss of Strat. Although these data indicate that adding one copy of *spdo* or *numb*, or removing one copy of *neur* in the *strat* mutant background, led to an increased activation of Notch pathway, future work is needed to determine whether activation could take place at the TGN or to identify the compartment from which activation takes place. It is also conceivable that the function of Strat/Rab8 is linked to subsequent Notch processing events, as reported in a recent study showing the importance of Rab8 localization in the proteolytic activation of Notch1 in mammals (Court et al., 2017).

Site of action of Strat/Rab8 and specificity to Notch

Our localization studies point to a function of Strat and Rab8 at the TGN. Loss of Strat or Rab8 caused the accumulation of Spdo in the TGN and its apical accumulation. This situation is somehow similar to what has been recently reported for basement membrane proteins in follicular epithelial cells in *Drosophila* (Devergne et al., 2017). Loss of Strat caused mis-secretion of type IV Collagen and Perlecan apically, indicating that Strat function is to restrict their deposition basally. Overexpressed Strat::HA was localized basally, but the exact compartments were not identified. However, and in contrast to Spdo/Notch, no intracellular accumulation of Collagen or Perlecan was reported. Nonetheless, their localization was monitored using GFP-tag. Interestingly, we here report for SpdoiGFP and Notch::GFP^{crispr} that the GFP signal was not fluorescent at the TGN. Thus, it will be important to determine whether Collagen and Perlecan also accumulate in the TGN as Notch and Spdo upon loss of Strat. This would further extend the notion that Strat/Rab8 control the packaging and sorting of cargoes other than Notch/Spdo in the TGN for basolateral targeting. In that respect, Strat is not selective to Notch signaling and further work is needed to decipher what is/are the molecular signature of cargoes recognized by Strat/Rab8.

Is Strat a GEF or a chaperone?

Whether Strat/Mss4 acts as a GEF (Burton et al., 1993, 1994; Moya et al., 1993; Itzen et al., 2006b; Zhu et al., 2001) or a chaperone (Gulbranson et al., 2017; Nuoffer et al., 1997; Wixler et al., 2011) is highly debated. Recently, Mss4 was also described as a Rab-stabilizing holdase chaperone (Gulbranson et al., 2017). Indeed, in HeLa cells CRISPR-depleted from Strat/Mss4, the closely related Rab8, Rab10 and Rrab13 are efficiently synthesized but undergo rapid proteasome degradation (Gulbranson et al., 2017). Here, in contrast to mammalian cells, we reported that the levels of Rab8 were unaffected by the loss of Strat, arguing that *Drosophila* Strat does not behave as a stabilizing holdase chaperone.

The fact that overexpressed wild-type Rab8 rescued *strat* as well as the constitutively active version of Rab8 is consistent with a model of Strat being a chaperone rather than a GEF. However, it is also conceivable that once overexpressed, there were sufficient amounts of wild-type Rab8 bound to GTP, independently of GEF activity, to bypass the requirements for Strat. It would thus be interesting to test whether a constitutively active version of Rab8 expressed at physiological levels could rescue Strat phenotypes. Such an experiment might be an essential step towards deciphering whether Strat functions as a GEF or not *in vivo*. We nonetheless observed that overexpression of the constitutively inactive form of Rab8 aggravated the Strat phenotype (27% of SOs transformed with 19% and 8% of *Notch* gain and loss of function, respectively, data not shown). This increased phenotype suggests that Rab8T22N titrated a GEF that normally activated the residual levels of Rab proteins and was still localized at the TGN upon loss of Strat. Because the mammalian Rab8 GEF, called Rabin8 GEF, has no *Drosophila* ortholog, the identification of possible *Drosophila* Rab8 GEF appears also to be crucial to better understanding Strat function.

Specificity of Strat towards Rab GTPases

Among the five Rabs predicted to interact with Strat, we found that Rab8, but not Rab1, Rab3 or Rab35, was mislocalized in *strat* cells. In addition to Rab8, we found that in large clones of cells mutant for *strat*, Rab10 localization was also affected. To test the possibility that Strat also regulates Rab10, we performed rescue experiments by overexpressing the catalytic active, GTP-bound form of Rab10 in *strat* clones. However, we found that overexpression of the GTP-bound form of Rab10 in a wild-type background resulted in a notum devoid of SOPs, as judged by the absence of Cut staining (data not shown). Although this experiment suggests that Rab10 activity might be required for the Notch-dependent selection of SOPs within the proneural clusters, it prevented us from testing whether Strat also regulates Rab10 activity in binary cell fate decision during ACD.

It is interesting to note that in follicular epithelial cells of *Drosophila* egg chamber, the GTP-bound form of Rab10 was unable to rescue the apical mislocalization of basement membrane components induced by silencing of *strat* (Devergne et al., 2017). Collectively, these results suggest that, depending on the tissue and cellular context, Strat could regulate the activity/localization of more than one Rab GTPase to fulfill its function. This would explain why homozygous *strat* mutant animals died at earlier stage and caused more penetrant *Notch* phenotypes than those observed in *rab8* mutant.

Similarities and differences in the polarized transport by Strat/Rab8 and the clathrin adaptor complex AP-1

The data showing that Strat/Rab8 control the packaging and sorting of cargoes within the TGN for basolateral targeting *in vivo* in *Drosophila* (this study; Devergne et al., 2017) are consistent with the role of Rab8 in the basolateral transport of some cargoes in mammals (Ang et al., 2003; Henry and Sheff, 2008; Huber et al., 1993). However, loss of Rab8 was also reported to regulate apical transport in mammals (Nakajo et al., 2016; Sato et al., 2014, 2007). Whether differences in cell types, cargoes or Rab8

Development (2018) 145, dev163469. doi:10.1242/dev.163469

effector(s) account for these apparent discrepancies in mammals is unclear at present.

Potential Rab8 effectors include the AP-1 complex. In mammals, Rab8 was reported to colocalize with the AP-1 complex where the overexpression of the catalytically active form of Rab8 caused the mislocalization of AP-1B complex and the selective misrouting of newly synthesized AP-1B-dependent cargo apically (Ang et al., 2003). In pupal notum, the loss of Rab8, Strat (this study) or AP-1 (Benhra et al., 2011) resulted in an apical accumulation of Spdo, raising the possibility that Rab8 and AP-1 could function in the same basolateral trafficking pathway in *Drosophila*. Epistasis analyses between Strat and AP-1 will be needed to determine whether Strat/Rab8 trafficking towards the basolateral membrane is direct or indirect via AP-1 and recycling endosomes (Benhra et al., 2011). In any case, both Strat/Rab8 and AP-1 are involved in restricting the apical delivery of Spdo to control in time and space Notch activation following ACD.

MATERIALS AND METHODS

Drosophila stocks and genetics

Drosophila melanogaster stocks were maintained and crossed at 25°C. Mitotic clones were induced using the FLP-FRT technique using the *hs*-FLP and by heat shocking (2×60 min at 37°C) at second and early third instar larvae. *pnr*-GAL4 was used to drive the expression of different forms of Rab proteins and for the Strat::HA construct, while the *neur*^{P72}-GAL4 driver was used to drive expression of UAS-Pon::GFP, UAS-*SpdoL2::mChFP* and UAS-*Spdo::Dendra2* constructs.

The following stocks were used in this study: *w; strat*/CyO (Fig. 1A), *w; strat*^{WT} (Fig. 1A), *w; strat*^{27,77,94}/CyO (Fig. 1A), *w; strat*^{HA}/CyO (Fig. 1A), *y, hs*-FLP*; Ubi-GFP nls,* FRT40A (Figs 1B,B′; 2A-C″; 3A-C; 3E; 4; 5B-C′; 6B,B′; 6C-E′; 6G; Figs S1A-B′; S3A,A′; S4A-C′; S4E,F; S5B-C and S6C,C′), *w; strat,* FRT40A/CyO (Figs 1B-D′; 2A-C″; 3A-C; 3E; 4; 5C,C′; 6B,B′; 6C-E′; 6G; Figs S1A-B′; S3A,A′; S4A-C′; S4E,F; S5B,C and S6C,C′), *tub*-GAL80*,* FRT40A*; neur*^{P72}-GAL4, UAS-Pon::GFP/SM6a*,* TM6 *Tb* (Fig. 1C-D′), *w; strat,* FRT40A/CyO*;* FRT82B*,* NumbGFP/TM6 *Tb* (Fig. 2A, Figs S2A-A″, S4D,D′ (Couturier et al., 2013), *y hs*-FLP*; Ubi-RFP nls*, FRT40A (Fig. 2D-D″, Figs S2A-A″, S3B,B′ and S4D,D′), *w; Numb::*GFP^{crispr}, FRT40A (Fig. 2D), *w; strat, Numb*::GFP^{crispr}, FRT40A/CyO (Fig. 2D′,D″), *y hs*-FLP*; strat,* FRT40A*; sqh-sqh::mCherry* (Figs 3D-F′; 6B,B′; Figs S1C,C′; S6A-D; Martin et al., 2009), *y hs*-FLP*; Ubi-RFP nls;* SpdoiGFP (Fig. 3D-F′; Couturier et al., 2013), *w; strat,* FRT40A/CyO; *neur*^{P72}-GAL4, UAS-*SpdoL2::mChFP*/TM6 *Tb* (Fig. 5B,B′; Benhra et al., 2011), *y w hs*-FLP*; Ubi-GFP nls,* FRT40A*; pnr*-GAL4/TM6 *Tb* (Fig. 6A,G and Fig. S6F-H), *w; strat,* FRT40A/CyO*;* UAS-*strat::HA*/(TM6 *Tb*) (Fig. 6A, a kind gift from T. Schüpbach, Princeton University, NJ, USA), *w*^{1118}*;; Rab8*^{EYFP} (Fig. S6C,C′), BL62546 (Dunst et al., 2015), W1118 (Fig. 6F and Fig. S6E), *w; strat,* FRT40A/CyO CFP (Fig. 6F and Fig. S6E), *y hs*-FLP*;; Ubi-GFP nls,* FRT80B (Fig. 7A,B, a kind gift from P. Thérond, Institut de Biologie Valrose, Nice, France), *w*^{1118}*;; rab8*^{U1}*,* FRT80B/TM6 *Tb Sb* (Fig. 7A-B, a kind gift from P. Thérond), *y w Baz::*GFP*; Ubi-RFP nls,* FRT40A/CyO (Fig. S1C,C′, Fly Trap line CC01941; Buszczak et al., 2007), *Notch::GFP*^{crispr}*; strat,* FRT40A/CyO (Fig. S3B,B′), *w; strat,* FRT40A/CyO; *neur*^{P72}-GAL4*,* UAS-*Spdo::Dendra2*/TM6 *Tb* (Fig. S5B-C), *w*^{1118}*;; Rab1*^{EYFP} (Fig. S6A), BL62539 (Dunst et al., 2015), *w*^{1118} *Rab35*^{EYFP} (Fig. S6B), BL62559 (Dunst et al., 2015), *w*^{1118} *Rab10*^{EYFP} (Fig. S6D), BL62548 (Dunst et al., 2015),

The following stocks from Bloomington were used:

w^{1118}, Df(2L)BSC200/CyO;

y^{1} *w*;* P{UASp-YFP.Rab8.Q67L}Sc2^{10}/TM3, P{Thb8-lacZ}WD1, *Sb*^{1} *Ser*^{1} (the constitutively active form of Rab8, Fig. 6G), BL23301;

y^{1} *w*;* P{UASp-YFP.Rab8}CG6175^{09}/TM3, *Sb*^{1} (the wild-type form of Rab8, Fig. 6G and Fig. S6F-H), BL23272;

y^{1} *w*;* P{UASp-YFP.Rab10.Q68L}27a (the constitutively active form of Rab10), BL9787; and

y^{1} *w*;* P{UASp-YFP.Rab35.Q67L}01/TM3, *Sb*^{1} (the constitutively active form of Rab35), BL9817.

Generation of *strat*

The *strat* mutant was generated using the CRISPR/Cas9 system. Following gRNAs were used: 5′-GACACAGT|GTGACCACTCAA CGG-3′ and 5′-GTCAGAAG|GGTTTAGCCGTT CGG-3′ to induce Cas9 cuts on each side of the exon 1 of Strat protein, three nucleotides upstream of the PAM site. Annealing of oligonucleotides, digestion of the pU6-*Bbs*I-chiRNA plasmid, ligation of annealed oligonucleotides and transformation were performed according to previously described protocols (Gratz et al., 2013a,b). According to the same protocol, homology arms were cloned in the pHD-Dsred-attP plasmid for homology-directed repair. Homology arm1 and homology arm2 measured, respectively, 2013 bp and 2014 bp. Injections were performed by BestGene, in vas-Cas9(X) RFP stock (stock BL#55821). To verify the correct position of the DsRed cassette, primers were designed upstream and downstream of homology arms and within the DsRed sequence. The following primers were used to verify the correct position of the DsRed cassette: 5′-GGGTTCTTGGCCTTTTGAGG-3′ and 5′-CCAGTTGGGGC-ACTACGAT-3′ to amplify arm1 and a part of the insertion; and 5′-TCAC-TGCATTCTAGTTGTGGT-3′ and 5′-AGCTGGACGGTACACAAGTA-3′ to amplify a part of the insertion and arm2.

Transgenic lines

Gene synthesis of *strat*^{WT}, *strat*^{27,77,94} and *strat*^{HA} were performed by GeneWizz. The syntheses are composed of the 5′ and 3′ untranslated regions and the coding region. In addition, for *strat*^{HA}, we added the following sequence corresponding to linkers and HA sequence: GCCGCCGTGTA-CCCCTACGACGTGCCCGACTACGCCCCCGCCGCC just before the stop codon [the HA sequence comes from Kumar et al. (2000)]. The gene products were inserted in the pRIV^{white} plasmid (Baena-Lopez et al., 2013) and phiC31 integrase-mediated site-specific transgenesis was performed by Bestgene in the *w; strat,* FRT40A/CyO stock. The cysteine 27, asparagine 77 and aspartate 94 residues were substituted with alanine according to Zhu et al. (2001). The *mini-white* was used as marker to identify flies where integration at the attP site occurred. Point mutations, the HA insertion and the correct integrations were verified by sequencing. For all lines, the following primers were used: 5′-TTTTGTTTGTAAGAACGGAAACG-3′ and 5′-TTTGTCGAGTTTAGATTTAAGCGA-3′ upstream and in the synthetized gene.

Numb::GFP^{crispr} was generated starting from the *numb*^{crispr} performed in the laboratory. For the *numb*^{crispr} the following gRNAs were used: 5′-GA-GCGAGA|GGGCTAGCGAACAGG-3′ and 5′-GAAGGATA|ACGAAGG-ACGCG AGG-3′ to induce Cas9 cuts upstream of the exon 1 and downstream of the exon 2, respectively. The protocol was the same as the one described for inserting *strat* into an attP landing site. Homology arms 1 and 2 measure 2001 bp and 2020 bp, respectively, and the following primers were used to verify the correct position of the DsRed cassette: 5′-CTGCCCATCTCGC-CATAAGA-3′ and 5′-GATGACGTCCTCGGAGGAGGC-3′ to amplify arm1 and part of the insertion; and 5′-ATCGTGGAGCAGTACGAGCG-3′ and 5′-TGGTGGACTTTCGTGGGTAA-3′ and to amplify a part of the insertion and arm2.

Numb-RA (5′ and 3′ untranslated regions and the coding region, CloneRE15808 from Berkeley Drosophila Genome Project) with the GFP inserted at the C-terminal of the protein (Couturier et al., 2013) was inserted into the pRIV^{white} plasmid (Baena-Lopez et al., 2013). PhiC31 integrase-mediated site-specific transgenesis was performed by Bestgene in *w; numb*^{crispr} attP, FRT40A/CyO stock. *mini-white* was used as genetic marker to identify flies in which integration at the attP site occurred.

For Notch::GFP^{crispr}, the following gRNAs were used: 5′-AACTTGAA|-TGGATTGAACCC GGG-3′ and 5′-CGAACTGG|AGGGTTCTCCTGT-TG-3′ to introduce Cas9 cuts in exon 6 and to introduce the GFP, flanked by GVG linkers, and the DsRed cassette, flanked by loxP, at the previously described position (NiYFP4) (Couturier et al., 2012). Homology arms 1 and 2 measure 1064 bp and 1263 bp. Injection was performed by Bestgene in the *yw*; attP40(nos-cas9)/Cyo stock. The correct position of the GFP and the DsRed cassette was verified by PCR and sequencing. The DsRed was then removed by crossings with *if*/Cyo Crew stock.

The UAS-*Spdo::Dendra2* construct was generated by a two-step PCR amplification to produce an in-frame fusion of Spdo to the Dendra2 fluorescent protein at its C-terminal region using the pUASt-*Spdo* vector

Development (2018) 145, dev163469. doi:10.1242/dev.163469

(a kind gift from J. Skeath, Washington University, St Louis, MO, USA) (O'Connor-Giles and Skeath, 2003) and the pDendra2-N1 vector (a kind gift from X. Darzacq, Ecole Normale Supérieure, Paris, France).

Immunofluorescence and antibodies

Pupae were aged for 16.5 to 18 h after puparium formation (APF) in order for SOPs to reach the two-cell stage) and aged for 24 h to 28 h APF (for lineage analyses), dissected in 1× phosphate-buffered saline (1× PBS) and then fixed for 15 min in 4% paraformaldehyde at room temperature. Dissection and staining conditions were essentially as previously described (Le Borgne and Schweisguth, 2003). Brains of larvae were dissected in 1× PBS, fixed for 20 min in 4% paraformaldehyde at room temperature, incubated with primary antibodies overnight at 4°C and with secondary antibodies for 2 h at room temperature. Primary antibodies used were mouse anti-Cut [2B10, Developmental Studies Hybridoma Bank (DSHB), 1:500], rat anti-Elav (7E10, DSHB, 1:200), goat anti-Su(H) (sc15813, Santa Cruz, 1:500), rat anti-DE-Cad (DCAD2, DSHB, 1:500), mouse anti-Dlg (4F3, DSHB, 1:500), goat anti-Numb (SC23579, Santa Cruz, 1:200), rabbit anti-Neuralized (a kind gift from E. Lai, Memorial Sloan Kettering Cancer Center, New York, USA) (Lai et al., 2001), 1:1000), rabbit anti-Spdo (a kind gift from J. Skeath) (O'Connor-Giles and Skeath, 2003) (1:2000), mouse anti-GFP (clone 7.1, Roche, 1:500), rabbit anti-GM130 (ab30637, Abcam, 1:1000), guinea pig anti-Spdo (a kind gift from J. Knoblich, IMBA-Institute of Molecular Biotechnology, Vienna, Austria) (Hutterer and Knoblich, 2005), 1:2000), rabbit anti-Syx16 (ab32340, Abcam, 1:1000), rabbit anti-AP-1γ (a kind gift from M. S. Robinson, Cambridge Institute for Medical Research, Cambridge, UK) (Hirst et al., 2009), 1:500), mouse anti-NICD (C17.9C6, DSHB, 1:200), mouse anti-DECD (C594.9B, DSHB, 1:200), mouse anti-Rab11 (610656, BD Biosciences, 1:100), mouse anti-HRS (27-4, DSHB, 1:100), mouse anti-HA (16B12, Covance, 1:1000) and mouse anti-Rab8 (610844, BD Biosciences, 1:500). Cy2-, Cy3- and Cy5-coupled secondary antibodies (1:400) were from Jackson's Laboratories and Phalloidin-Alexa-547 was from from Life Technologies (1:500).

Imaging

Images were acquired with a LSM Leica SPE confocal microscope for fixed nota, MARCM experiments, live imaging of SpdoiGFP and Numb::GFP^{crispr}, and fixed brains. All images were processed and assembled using ImageJ 1.48 and Adobe Illustrator.

Quantification of the enrichment of Spdo at the apical level

The fluorescence intensity was calculated using the same method for wild-type and *strat* two-cell stages. With ImageJ software, a *z* projection of the two most apical planes (sum slices function) was carried out and the average fluorescence intensity on a hand-drawn area encompassing the apical SO surface was calculated. Then, the values of the background noise calculated on the same *z* projection with the same hand-drawn area were substracted.

Colocalization measurement

The colocalization test between proteins was measured using the Icy Software (icy.bioimageanalysis.org; de Chaumont et al., 2012). Measures were carried out on segmented images of two-cell stages (17 h-17.5 h APF) using Active Contours plug-in, Protocols plug-ins and ImageJ 1.48 to take into account the signal coming from only the two cells. The C-CRAFT and GcoPS algorithms were used to segment intracellular structures and to calculate the colocalization test, respectively. For the Rab8 and GM130 data, we applied the same threshold on all images of Rab8 to eliminate the noise, then we applied the GM130 signal as a mask on these images of Rab8 in order to calculate the colocalization test between Rab8 and GM130 in only Golgi structures.

Cell-surface labeling and antibody-uptake experiments

For the pulse-chase internalization experiment, pupal nota were dissected in Schneider's *Drosophila* medium (Gibco-BRL) containing 5% fetal calf serum (Gibco-BRL). After dissection, pupal nota were incubated with rabbit anti-RFP antibody (PM005, MBL, 1:400) and mouse anti-Delta antibody (DECD C594-9B, DSHB, 1:200) for 10 min on ice (cell surface staining), washed with Schneider's *Drosophila* medium and then incubated at room temperature for 15 min before washing and fixation. Localization of RFP and Delta was then revealed using secondary antibodies.

Photoconversion assay

Photoconversion experiments were performed on living pupa at the two-cell stages (17 h-17.5 h APF at 25°C) using a Leica SP8 confocal microscope equipped with a 63× objective and a 405 nm laser. For each experiment, eight points were drawn at apical level of mutant cells in the plane where Spdo is most enriched. For the photoconversion the 405 nm laser was used at 0.5% intensity and images were acquired only in this apical plane with a minimum frame interval of 2.58 s.

Western blotting analysis

Five and three brains of *strat* and wild-type larvae, respectively, were dissected in 1× PBS. Samples were immediately stored in Laemmli buffer at −20°C to avoid protein degradation. After denaturation, samples were loaded on a 14% denaturing SDS-polyacrylamide gel and then transferred on a nitrocellulose membrane (GE Healthcare, Life Sciences). The following primary antibodies were used: mouse anti-Rab8 (610844, BD Biosciences, 1:4000) and rat anti-αTubulin (MAB1864, EMD Millipore, 1:1000), followed horseradish peroxidase-conjugated anti-mouse and anti-rat antibodies (112-035-003 for anti-rat and 115-035-003 for anti-mouse, Jackson's Laboratories, 1:10,000). Membranes were incubated with the SuperSignal West Pico Chemiluminescent Substrate from Thermo Fisher Scientific. Whole membranes are shown in Fig. S4.

Statistical analysis

Statistical analysis was carried out using the R software version 3.3.3. A Shapiro test was used to determine the normal distribution of data. According to the distribution, we then performed an ANOVA or a Wilcoxon test. Statistical significances are represented as follows: *P<0.05; **P<0.01 and ***P<0.001.

Acknowledgements

We thank P. Thérond for sharing the *rab8^{U1}* allele prior to publication, and Y. Hong, F. Schweisguth, T. Schüpbach, the Bloomington Stock Center, the Vienna Drosophila RNAi Center, the TRiP at Harvard Medical School (NIH/NIGMS R01-GM084947) and the National Institute of Genetics Fly Stock Center for providing fly stocks. We also thank P. Uhart for the generation and characterization of the UAS-Sanpodo::Dendra2 transgenic line and the generation of the *numb*^{crispr} attP founder line *notch::GFP*^{crispr}, and S. Dutertre and C. Chevalier from the Microscopy Rennes Imaging Center-BIOSIT (France). The monoclonal antibodies against Cut, Dlg, E-Cad and Elav were obtained from the Developmental Studies Hybridoma Bank, generated under the auspices of the National Institute of Child Health and Human Development, and maintained by the University of Iowa Department of Biological Sciences. We thank A. Bardin, G. Bertolin, A. Echard, S. Miserey-Lenkei and members of R.L.B.'s laboratory for helpful discussions and critical reading of the manuscript. We also thank A. Rouaze, from InDroso (Biosit, University of Rennes, France), for helpful discussions and sharing reagents for the CRISPR/Cas9 method.

Competing interests

The authors declare no competing or financial interests.

Author contributions

Conceptualization: K.B., R.L.B.; Methodology: K.B., I.G., R.L.B.; Formal analysis: K.B.; Investigation: K.B.; Resources: K.B., I.G.; Writing - original draft: K.B.; Writing - review & editing: K.B., R.L.B.; Visualization: K.B., R.L.B.; Supervision: R.L.B.; Project administration: R.L.B.; Funding acquisition: R.L.B.

Funding

This work was supported in part by the ARED programme from the Région Bretagne/Agence Nationale de la Recherche (ANR-16-CE13-004-01 to K.B.), the Fondation pour la Recherche Médicale (FDT20170436864 to K.B.), La Ligue contre le Cancer-Equipe Labellisée (R.L.B.) and the Association Nationale de la Recherche et de la Technologie programme PRC Vie, santé et bien-être CytoSIGN (ANR-16-CE13-004-01 to R.L.B.).

Supplementary information

Supplementary information available online at
http://dev.biologists.org/lookup/doi/10.1242/dev.163469.supplemental

References

Ang, A. L., Fölsch, H., Koivisto, U.-M., Pypaert, M. and Mellman, I. (2003). The Rab8 GTPase selectively regulates AP-1B-dependent basolateral transport in polarized Madin-Darby canine kidney cells. *J. Cell Biol.* **163**, 339-350.

Baena-Lopez, L. A., Alexandre, C., Mitchell, A., Pasakarnis, L. and Vincent, J.-P. (2013). Accelerated homologous recombination and subsequent genome modification in Drosophila. *Development* **140**, 4818-4825.

Benhra, N., Lallet, S., Cotton, M., Le Bras, S., Dussert, A. and Le Borgne, R. (2011). AP-1 controls the trafficking of Notch and Sanpodo toward E-Cadherin junctions in sensory organ precursors. *Curr. Biol.* **21**, 1-9.

Bischof, J., Maeda, R. K., Hediger, M., Karch, F. and Basler, K. (2007). An optimized transgenesis system for Drosophila using germ-line-specific phiC31 integrases. *Proc. Natl. Acad. Sci. USA* **104**, 3312-3317.

Bray, S. (1998). Notch signalling in Drosophila: three ways to use a pathway. *Semin. Cell Dev. Biol.* **9**, 591-597.

Burton, J., Roberts, D., Montaldi, M., Novick, P. and De Camilli, P. (1993). A mammalian guanine-nucleotide-releasing protein enhances function of yeast secretory protein Sec4. *Nature* **361**, 464-467.

Burton, J. L., Burns, M. E., Gatti, E., Augustine, G. J. and De Camilli, P. (1994). Specific interactions of Mss4 with members of the Rab GTPase subfamily. *EMBO J.* **13**, 5547-5558.

Buszczak, M., Paterno, S., Lighthouse, D., Bachman, J., Planck, J., Owen, S., Skora, A. D., Nystul, T. G., Ohlstein, B., Allen, A. et al. (2007). The carnegie protein trap library: a versatile tool for Drosophila developmental studies. *Genetics* **175**, 1505-1531.

Cotton, M., Benhra, N. and Le Borgne, R. (2013). Numb inhibits the recycling of Sanpodo in Drosophila sensory organ precursor. *Curr. Biol.* **23**, 581-587.

Coumailleau, F., Fürthauer, M., Knoblich, J. A. and González-Gaitán, M. (2009). Directional Delta and Notch trafficking in Sara endosomes during asymmetric cell division. *Nature* **458**, 1051-1055.

Court, H., Ahearn, I. M., Amoyel, M., Bach, E. A. and Philips, M. R. (2017). Regulation of NOTCH signaling by RAB7 and RAB8 requires carboxyl methylation by ICMT. *J. Cell Biol.* **216**, 4165-4182.

Couturier, L., Vodovar, N. and Schweisguth, F. (2012). Endocytosis by Numb breaks Notch symmetry at cytokinesis. *Nat. Cell Biol.* **14**, 131-139.

Couturier, L., Mazouni, K. and Schweisguth, F. (2013). Numb localizes at endosomes and controls the endosomal sorting of notch after asymmetric division in Drosophila. *Curr. Biol.* **23**, 588-593.

Couturier, L., Trylinski, M., Mazouni, K., Darnet, L. and Schweisguth, F. (2014). A fluorescent tagging approach in Drosophila reveals late endosomal trafficking of Notch and Sanpodo. *J. Cell Biol.* **207**, 351-363.

de Chaumont, F., Dallongeville, S., Chenouard, N., Herve, N., Pop, S., Provoost, T., Meas-Yedid, V., Pankajakshan, P., Lecomte, T., Le Montagner, Y. et al. (2012). Icy: an open bioimage informatics platform for extended reproducible research. *Nat. Methods* **9**, 690-696.

Devergne, O., Sun, G. H. and Schüpbach, T. (2017). Stratum, a homolog of the human GEF Mss4, partnered with Rab8, controls the basal restriction of basement membrane proteins in epithelial cells. *Cell Rep.* **18**, 1831-1839.

Dunst, S., Kazimiers, T., von Zadow, F., Jambor, H., Sagner, A., Brankatschk, B., Mahmoud, A., Spannl, S., Tomancak, P., Eaton, S. et al. (2015). Endogenously tagged rab proteins: a resource to study membrane trafficking in Drosophila. *Dev. Cell* **33**, 351-365.

Fortini, M. E. and Bilder, D. (2009). Endocytic regulation of Notch signaling. *Curr. Opin. Genet. Dev.* **19**, 323-328.

Fürthauer, M. and González-Gaitán, M. (2009). Endocytic regulation of notch signalling during development. *Traffic* **10**, 792-802.

Gillingham, A. K., Sinka, R., Torres, I. L., Lilley, K. S. and Munro, S. (2014). Toward a comprehensive map of the effectors of rab GTPases. *Dev. Cell* **31**, 358-373.

Gratz, S. J., Cummings, A. M., Nguyen, J. N., Hamm, D. C., Donohue, L. K., Harrison, M. M., Wildonger, J. and O'Connor-Giles, K. M. (2013a). Genome engineering of Drosophila with the CRISPR RNA-guided Cas9 nuclease. *Genetics* **194**, 1029-1035.

Gratz, S. J., Wildonger, J., Harrison, M. M. and O'Connor-Giles, K. M. (2013b). CRISPR/Cas9-mediated genome engineering and the promise of designer flies on demand. *Fly (Austin)* **7**, 249-255.

Gulbranson, D. R., Davis, E. M., Demmitt, B. A., Ouyang, Y., Ye, Y., Yu, H. and Shen, J. (2017). RABIF/MSS4 is a Rab-stabilizing holdase chaperone required for GLUT4 exocytosis. *Proc. Natl. Acad. Sci. USA* **114**, E8224-E8233.

Guruharsha, K. G., Rual, J.-F., Zhai, B., Mintseris, J., Vaidya, P., Vaidya, N., Beekman, C., Wong, C., Rhee, D. Y., Cenaj, O. et al. (2011). A protein complex network of Drosophila melanogaster. *Cell* **147**, 690-703.

Hartenstein, V. and Posakony, J. W. (1989). Development of adult sensilla on the wing and notum of Drosophila melanogaster. *Development* **107**, 389-405.

Henry, L. and Sheff, D. R. (2008). Rab8 regulates basolateral secretory, but not recycling, traffic at the recycling endosome. *Mol. Biol. Cell* **19**, 2059-2068.

Hirst, J., Sahlender, D. A., Choma, M., Sinka, R., Harbour, M. E., Parkinson, M. and Robinson, M. S. (2009). Spatial and functional relationship of GGAs and AP-1 in Drosophila and HeLa cells. *Traffic* **10**, 1696-1710.

Huber, L. A., Pimplikar, S., Parton, R. G., Virta, H., Zerial, M. and Simons, K. (1993). Rab8, a small GTPase involved in vesicular traffic between the TGN and the basolateral plasma membrane. *J. Cell Biol.* **123**, 35-45.

Hutterer, A. and Knoblich, J. A. (2005). Numb and alpha-Adaptin regulate Sanpodo endocytosis to specify cell fate in Drosophila external sensory organs. *EMBO Rep.* **6**, 836-842.

Itzen, A., Bleimling, N., Ignatev, A., Pylypenko, O. and Rak, A. (2006a). Purification, crystallization and preliminary X-ray crystallographic analysis of mammalian MSS4-Rab8 GTPase protein complex. *Acta Crystallogr. Sect. F Struct. Biol. Cryst. Commun.* **62**, 113-116.

Itzen, A., Pylypenko, O., Goody, R. S., Alexandrov, K. and Rak, A. (2006b). Nucleotide exchange via local protein unfolding–structure of Rab8 in complex with MSS4. *EMBO J.* **25**, 1445-1455.

Johnson, S. A., Zitserman, D. and Roegiers, F. (2016). Numb regulates the balance between Notch recycling and late-endosome targeting in Drosophila neural progenitor cells. *Mol. Biol. Cell* **27**, 2857-2866.

Kondylis, V., Goulding, S. E., Dunne, J. C. and Rabouille, C. (2001). Biogenesis of Golgi stacks in imaginal discs of Drosophila melanogaster. *Mol. Biol. Cell* **12**, 2308-2327.

Kopan, R. and Ilagan, M. X. G. (2009). The canonical Notch signaling pathway: unfolding the activation mechanism. *Cell* **137**, 216-233.

Kumar, A., des Etages, S. A., Coelho, P. S. R., Roeder, G. S. and Snyder, M. (2000). High-throughput methods for the large-scale analysis of gene function by transposon tagging. *Methods Enzymol.* **328**, 550-574.

Lai, E. C. (2004). Notch signaling: control of cell communication and cell fate. *Development* **131**, 965-973.

Lai, E. C., Deblandre, G. A., Kintner, C. and Rubin, G. M. (2001). Drosophila neuralized is a ubiquitin ligase that promotes the internalization and degradation of delta. *Dev. Cell* **1**, 783-794.

Langevin, J., Le Borgne, R., Rosenfeld, F., Gho, M., Schweisguth, F. and Bellaïche, Y. (2005). Lethal giant larvae controls the localization of notch-signaling regulators numb, neuralized, and Sanpodo in Drosophila sensory-organ precursor cells. *Curr. Biol.* **15**, 955-962.

Le Borgne, R. and Schweisguth, F. (2003). Unequal segregation of Neuralized biases Notch activation during asymmetric cell division. *Dev. Cell* **5**, 139-148.

Le Borgne, R., Bardin, A. and Schweisguth, F. (2005). The roles of receptor and ligand endocytosis in regulating Notch signaling. *Development* **132**, 1751-1762.

Le Bras, S., Rondanino, C., Kriegel-Taki, G., Dussert, A. and Le Borgne, R. (2012). Genetic identification of intracellular trafficking regulators involved in notch-dependent binary cell fate acquisition following asymmetric cell division. *J. Cell Sci.* **125**, 4886-4901.

Lee, T. and Luo, L. (1999). Mosaic analysis with a repressible cell marker for studies of gene function in neuronal morphogenesis. *Neuron* **22**, 451-461.

Martin, A. C., Kaschube, M. and Wieschaus, E. F. (2009). Pulsed contractions of an actin-myosin network drive apical constriction. *Nature* **457**, 495-499.

Mavor, L. M., Miao, H., Zuo, Z., Holly, R. M., Xie, Y., Loerke, D. and Blankenship, J. T. (2016). Rab8 directs furrow ingression and membrane addition during epithelial formation in Drosophila melanogaster. *Development* **143**, 892-903.

Moya, M., Roberts, D. and Novick, P. (1993). DSS4-1 is a dominant suppressor of sec4-8 that encodes a nucleotide exchange protein that aids Sec4p function. *Nature* **361**, 460-463.

Nakajo, A., Yoshimura, S., Togawa, H., Kunii, M., Iwano, T., Izumi, A., Noguchi, Y., Watanabe, A., Goto, A., Sato, T. et al. (2016). EHBP1L1 coordinates Rab8 and Bin1 to regulate apical-directed transport in polarized epithelial cells. *J. Cell Biol.* **212**, 297-306.

Nuoffer, C., Wu, S. K., Dascher, C. and Balch, W. E. (1997). Mss4 does not function as an exchange factor for Rab in endoplasmic reticulum to Golgi transport. *Mol. Biol. Cell* **8**, 1305-1316.

O'Connor-Giles, K. M. and Skeath, J. B. (2003). Numb inhibits membrane localization of Sanpodo, a four-pass transmembrane protein, to promote asymmetric divisions in Drosophila. *Dev. Cell* **5**, 231-243.

Perdigoto, C. N. L. R., Gervais, L., Overstreet, E., Fischer, J., Guichet, A. and Schweisguth, F. (2008). Overexpression of partner of numb induces asymmetric distribution of the PI4P 5-Kinase Skittles in mitotic sensory organ precursor cells in Drosophila. *PLoS ONE* **3**, e3072.

Rajan, A., Tien, A.-C., Haueter, C. M., Schulze, K. L. and Bellen, H. J. (2009). The Arp2/3 complex and WASp are required for apical trafficking of Delta into microvilli during cell fate specification of sensory organ precursors. *Nat. Cell Biol.* **11**, 815-824.

Rhyu, M. S., Jan, L. Y. and Jan, Y. N. (1994). Asymmetric distribution of numb protein during division of the sensory organ precursor cell confers distinct fates to daughter cells [see comments]. *Cell* **76**, 477-491.

Sato, T., Mushiake, S., Kato, Y., Sato, K., Sato, M., Takeda, N., Ozono, K., Miki, K., Kubo, Y., Tsuji, A. et al. (2007). The Rab8 GTPase regulates apical protein localization in intestinal cells. *Nature* **448**, 366-369.

Sato, T., Iwano, T., Kunii, M., Matsuda, S., Mizuguchi, R., Jung, Y., Hagiwara, H., Yoshihara, Y., Yuzaki, M., Harada, R. et al. (2014). Rab8a and Rab8b are essential for several apical transport pathways but insufficient for ciliogenesis. *J. Cell Sci.* **127**, 422-431.

Development (2018) 145, dev163469. doi:10.1242/dev.163469

Tong, X., Zitserman, D., Serebriiskii, I., Andrake, M., Dunbrack, R. and Roegiers, F. (2010). Numb independently antagonizes Sanpodo membrane targeting and Notch signaling in Drosophila sensory organ precursor cells. *Mol. Biol. Cell* **21**, 802-810.

Trylinski, M., Mazouni, K. and Schweisguth, F. (2017). Intra-lineage fate decisions involve activation of Notch receptors basal to the midbody in Drosophila sensory organ precursor cells. *Curr. Biol.* **27**, 2239-2247.e3.

Upadhyay, A., Kandachar, V., Zitserman, D., Tong, X. and Roegiers, F. (2013). Sanpodo controls sensory organ precursor fate by directing Notch trafficking and binding gamma-secretase. *J. Cell Biol.* **201**, 439-448.

Wixler, V., Wixler, L., Altenfeld, A., Ludwig, S., Goody, R. S. and Itzen, A. (2011). Identification and characterisation of novel Mss4-binding Rab GTPases. *Biol. Chem.* **392**, 239-248.

Xu, H., Boulianne, G. L. and Trimble, W. S. (2002). Drosophila syntaxin 16 is a Q-SNARE implicated in Golgi dynamics. *J. Cell Sci.* **115**, 4447-4455.

Yamamoto, S., Charng, W.-L. and Bellen, H. J. (2010). Endocytosis and intracellular trafficking of Notch and its ligands. *Curr. Top. Dev. Biol.* **92**, 165-200.

Zhu, Z., Dumas, J. J., Lietzke, S. E. and Lambright, D. G. (2001). A helical turn motif in Mss4 is a critical determinant of Rab binding and nucleotide release. *Biochemistry* **40**, 3027-3036.

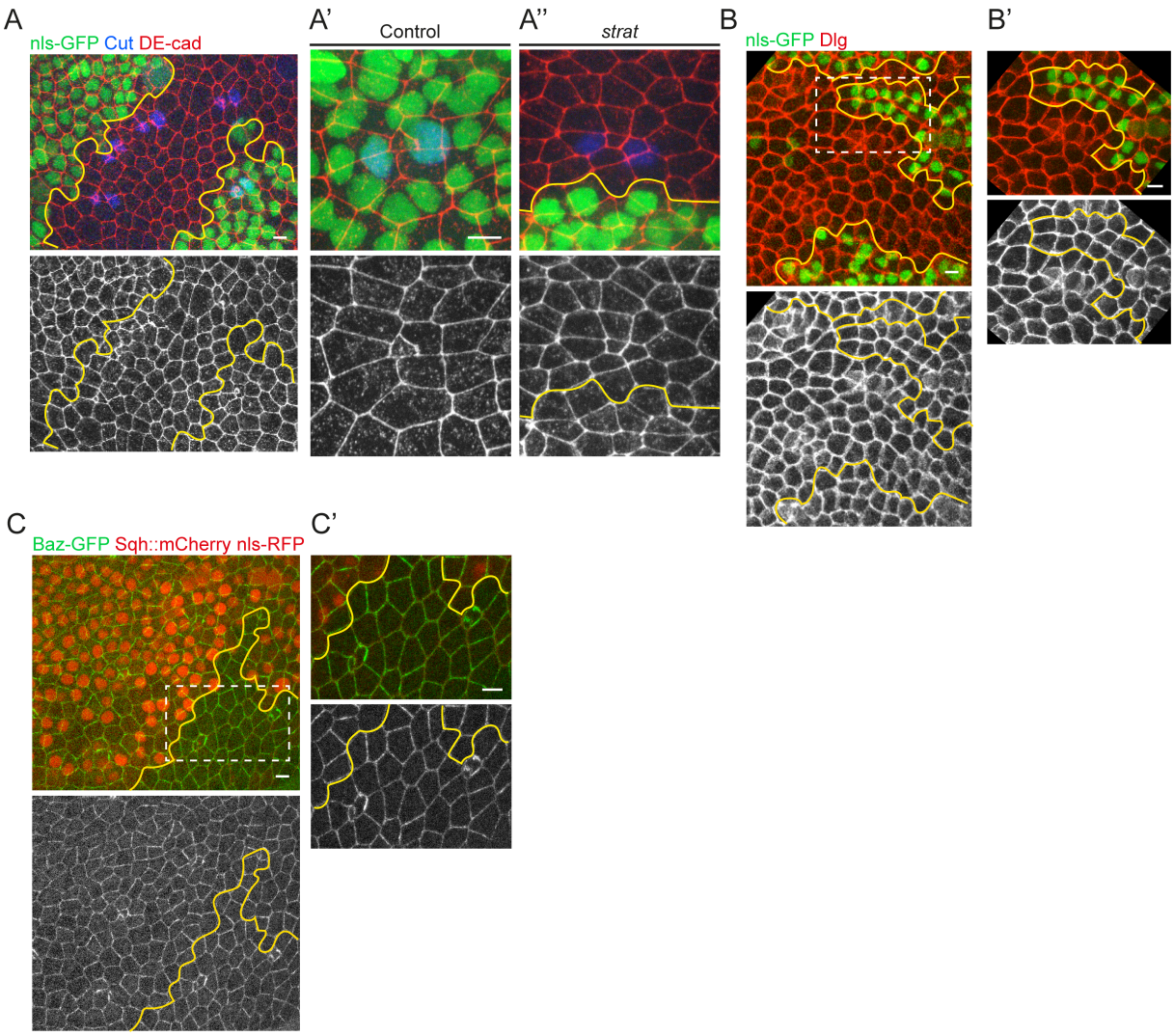

Figure S1: Localization of E-Cadherin, Par3/Baz and Dlg localization upon loss of Strat

A-A''. Localization of Cut (anti-Cut, blue) and E-cadherin (anti-DE-Cad, red). Panels show a high magnification of wild-type (**A'**) and *strat* SOP daughter cells (**A''**). **B-B'.** Localization of Dlg (anti-Dlg, red). The dashed white rectangle indicates the high magnification shown in **B'**. **C-C'.** Localization of Baz (Baz-GFP, green) and Myosin (Sqh::mCherry, red). The dashed white rectangle indicates the high magnification shown in **C'**. Wild-type and *strat* cells are separated by a yellow line. Scale bar is 5 μm.

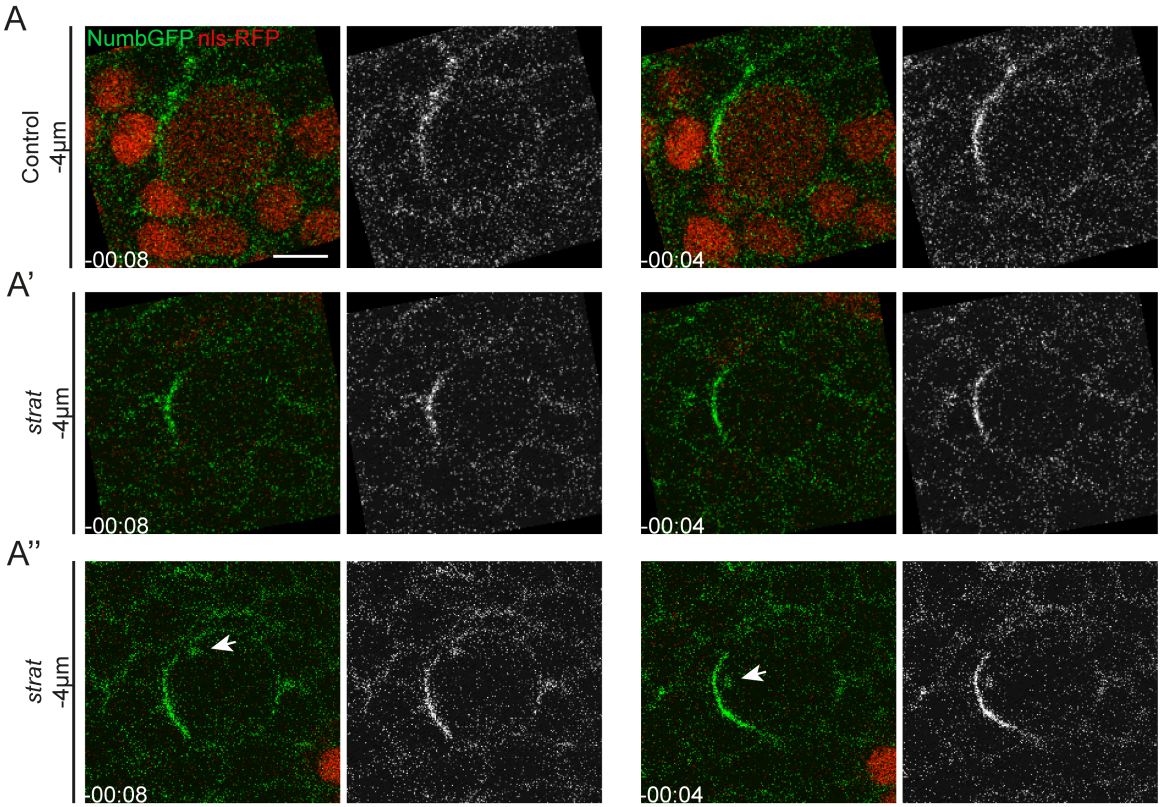

Figure S2: Unequal partitioning of extra copy NumbGFP in *strat* SOP

A-A''. Localization of NumbGFP (BAC rescue Construct (Couturier et al, 2013)) in wild-type SOP (**A**, n=9) and *strat* SOPs (**A'**, n=12/16 and **A''**, n=4/16). The white arrowhead indicates the cytoplasmic structure labeled with NumbGFP. Time is in hour:minute and the time 00:00. Scale bar is 5 µm.

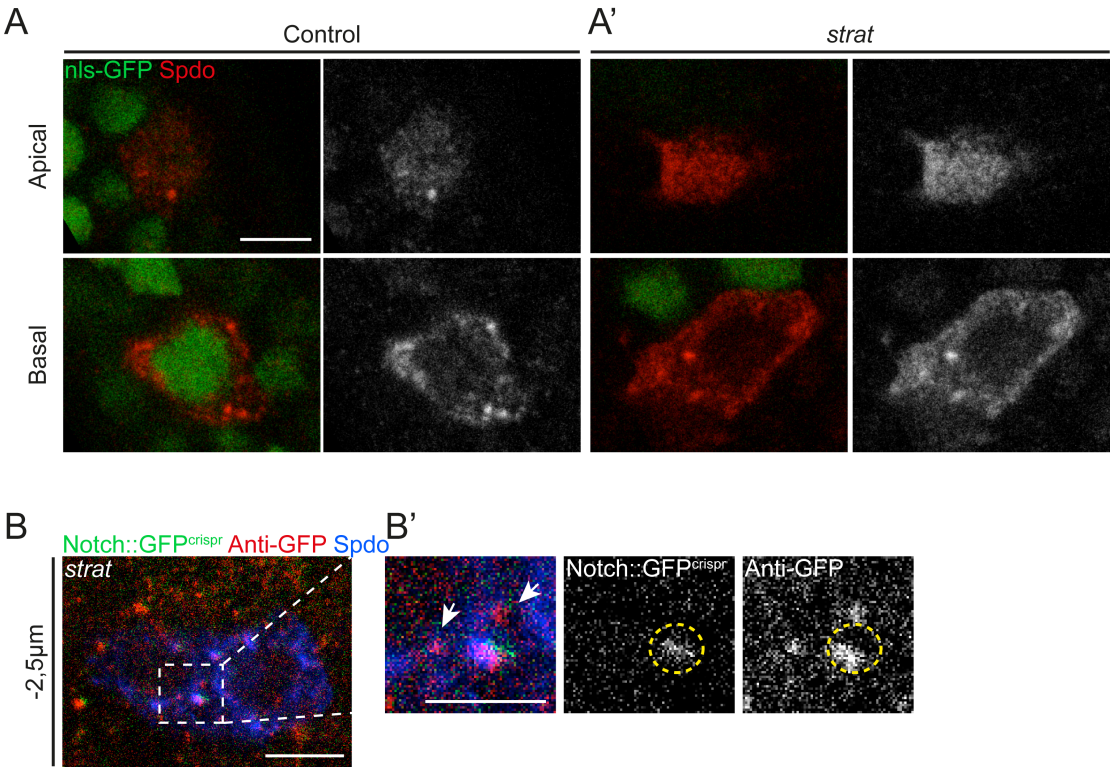

Figure S3: Strat controls the localization of Spdo and Notch in the SOP

A-A'. Localization of Spdo (anti-Spdo, red) in wild-type (**A**) and *strat* interphase SOPs (**A'**). *strat* mutant SO were identified by the loss of nls-GFP. **B.** Immunostainings of Notch::GFP^{crispr} (Notch::GFP^{crispr}, green and anti-GFP, red) and Spdo (anti-Spdo, blue) in *strat* SOP daughter cells. The dashed white rectangle delineates the high magnification (electronic zoom) shown in **B'**. The dashed yellow circle surrounds intracellular compartments positive for both Notch::GFP^{crispr} and anti-GFP. White arrowheads indicate intracellular compartments only positive for anti-GFP. Scale bar is 5 µm and 3 µm for the high magnification.

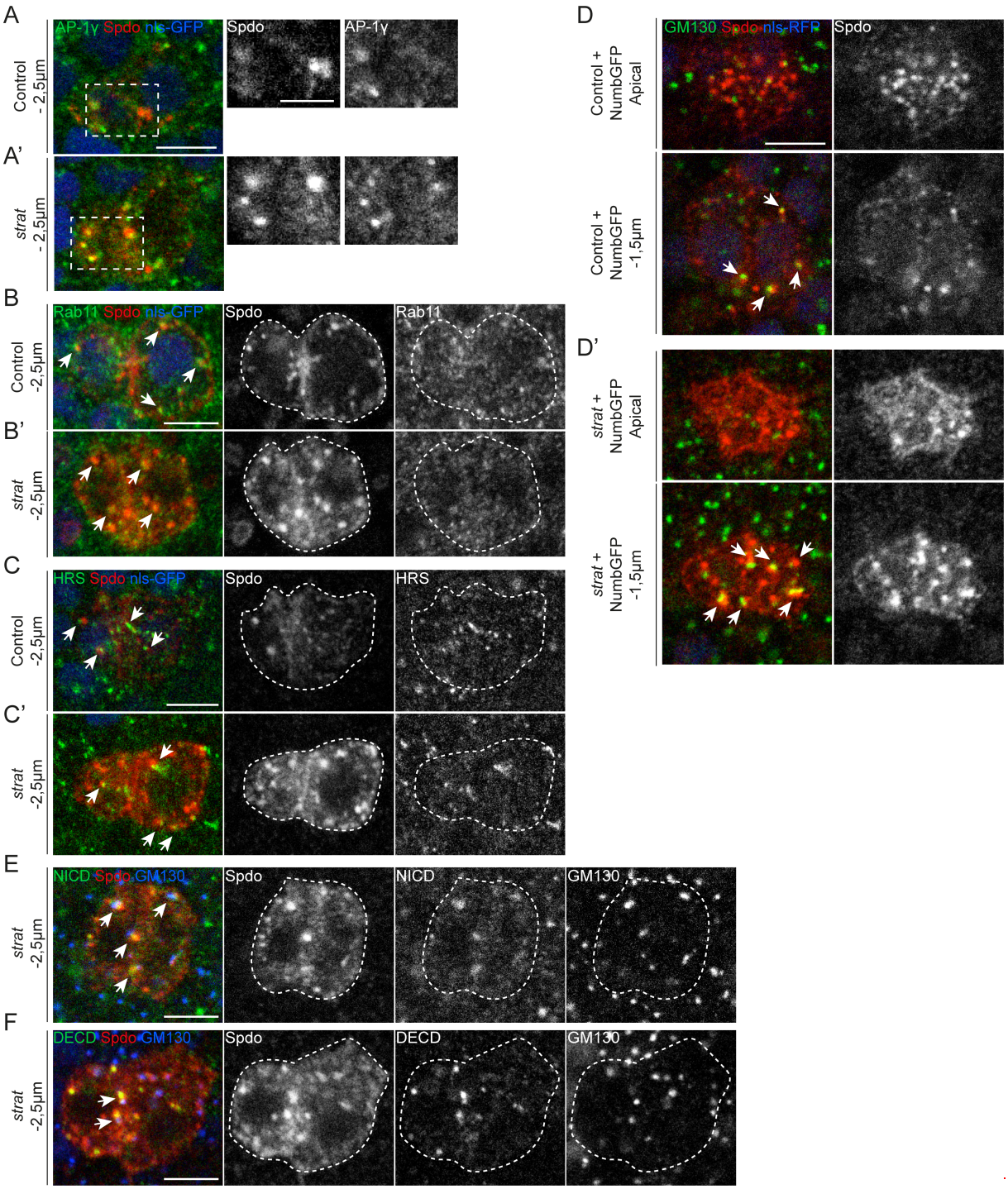

Figure S4: Loss of Strat causes accumulation of Spdo, Notch and Delta in the Golgi apparatus

A-A'. Localization of Spdo (anti-Spdo, red) and the *trans*-Golgi marker AP-1 (anti-AP-1γ, green) in wild-type (**A**) and *strat* SOP daughter cells (**A'**). The white dotted rectangles delineate the high magnification (electronic zoom) shown in right panels. **B-B'.** Localization of Spdo (anti-Spdo, red) and the marker of recycling endosomes Rab11 (anti-Rab11, green) in wild-type (**B**) and *strat* SOP daughter cells (**B'**). **C-C'.**

Localization of Spdo (anti-Spdo, red) and the endosomal marker HRS (anti-HRS, green) in wild-type (**C**) and *strat* SOP daughter cells (**C'**). **D-D'.** Localization of Spdo (anti-Spdo, red) and GM130 (anti-GM130, green) in wild-type (**D**) and *strat* SOP daughter cells expressing extra copy NumbGFP (**D'**). **E.** Localization of Spdo (anti-Spdo, red), Notch (anti-NICD, green) and GM130 (anti-GM130, blue) in *strat* SOP daughter cells. **F.** Localization of Spdo (anti-Spdo, red), Delta (anti-DECD, green) and GM130 (anti-GM130, blue) in *strat* SOP daughter cells. For each panel, white arrowheads indicate intracellular compartments positive for Spdo and other markers, and dashed white lines highlight the two-cell stage boundaries. *strat* mutant cells were identified by the loss of nls-GFP. Scale bar is 5 μm.

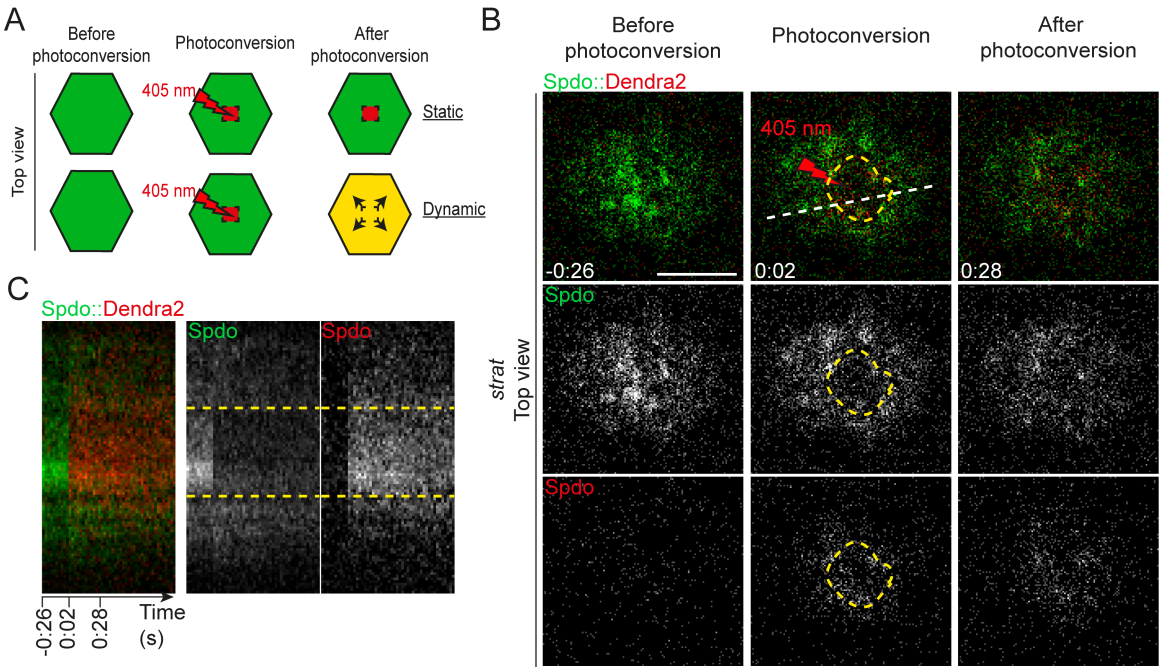

Figure S5: The apical pool of Spdo is highly dynamic in *strat*

A. Schematic representation of the photoconversion experiment in *strat*. The apical pool of Spdo::Dendra2 is represented in green and the photoconverted ROI is represented with dashed black squares. The photoconverted Spdo::Dendra2 (red) may be static and remain in the ROI or may be dynamic and diffuse outside the ROI (yellow). **B.** Time-lapse imaging of Spdo::Dendra2 in *strat* SOP daughter cells at the apical plane (n=29). Spdo::Dendra2 (green) is photoconverted in the ROI surrounded by a dashed yellow line. Time is in minute:second and the time 00:00 corresponds to the photoconversion. Scale bar is 3 µm. **C.** Kymographs representing the photoconversion of Spdo::Dendra2 along the dashed white line drawed in **B**. The photoconverted area is delimited with dashed yellow lines.

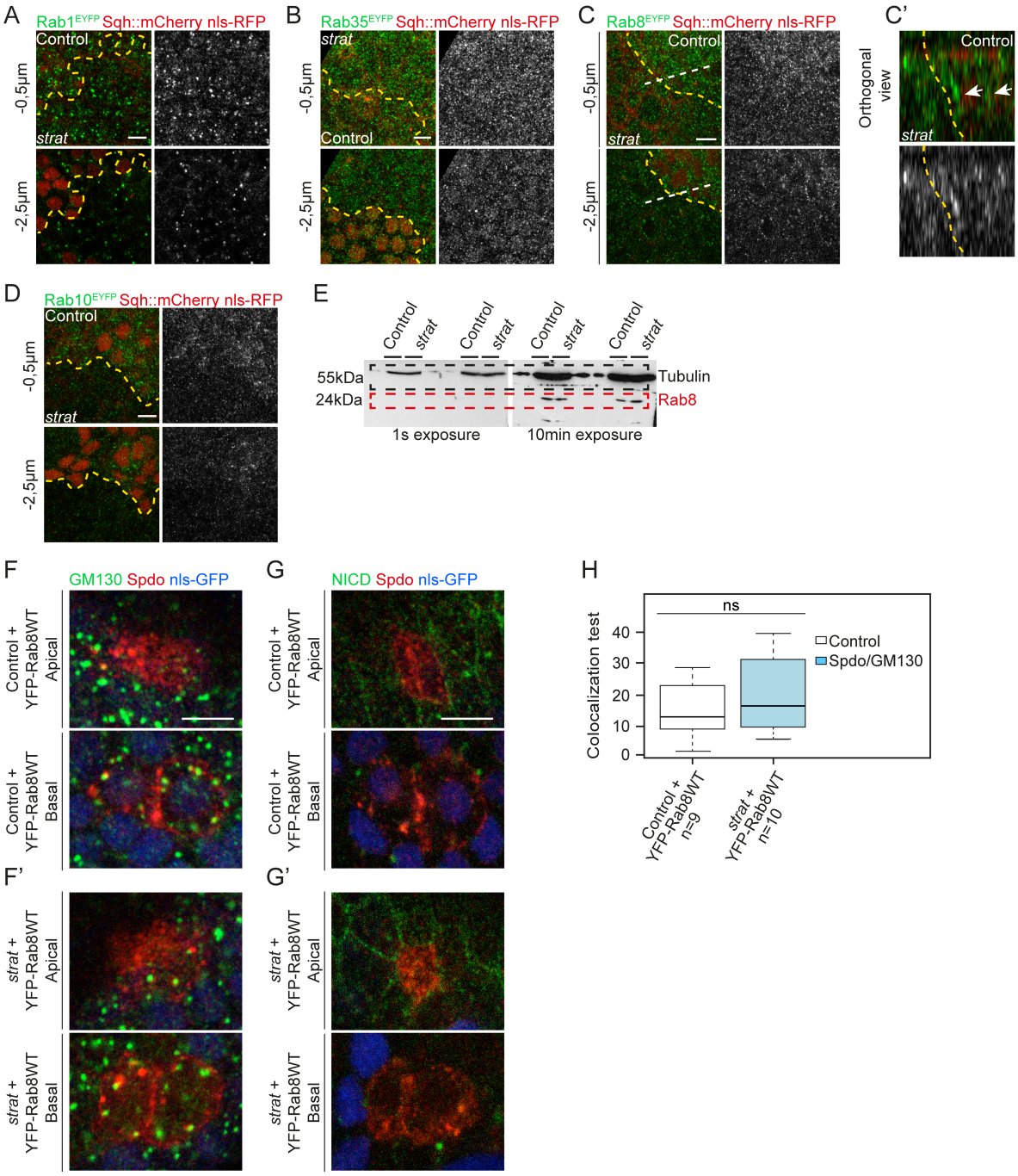

Figure S6: Strat regulates the localization Rab8 and Rab10 but not that of Rab1, Rab11 or Rab35

A-D. Localization of Rab1 (anti-GFP, Rab1^{EYFP}, green, **A**); Rab35 (anti-GFP, Rab35^{EYFP}, green, **B**); Rab8 (anti-GFP, Rab8^{EYFP}, green, **C**); Rab10 (anti-GFP, Rab10^{EYFP}, green, **D**); Myosin (Sqh::mCherry, red) and nls-RFP (used to identify wild-type cells) in nota of pupae. Wild-type and *strat* cells are separated by a dashed yellow line. Orthogonal sections along the dashed white line in **C** are shown in **C'**. White arrowheads show the localization of Rab8. **E.** Whole membranes of Western Blots showing Rab8 level (surrounded by a dashed red line) in brains of wild-type

and *strat* larvae after 1s exposure and 10min exposure. Tubulin was used as a loading control (surrounded by a dashed black line). **F-F'.** Localisation of Spdo (anti-Spdo, red) and GM130 (anti-GM130, green) in wild-type (**F**) and *strat* SOP daughter cells expressing YFP-Rab8WT (**F'**). **G-G'.** Localisation of Spdo (anti-Spdo, red) and Notch (anti-NICD, green) in wild-type (**G**) and *strat* SOP daughter cells expressing YFP-Rab8WT (**G'**). Scale bar is 5 μm. **H.** Box plots showing the colocalization between Spdo and GM130 in wild-type and *strat* SOP daughter cells expressing YFP-Rab8WT (ns, not significant, p-value>0.05).

Supplemental movies

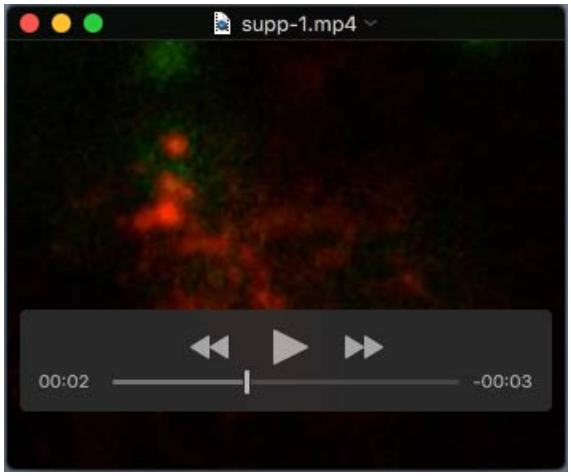

Movie S1: Spdo localization in wild-type SOP daughter cells

Localization of Spdo in wild-type SOP daughter cells from the apical pole to the basal pole (anti-Spdo, red and nls-GFP, green).

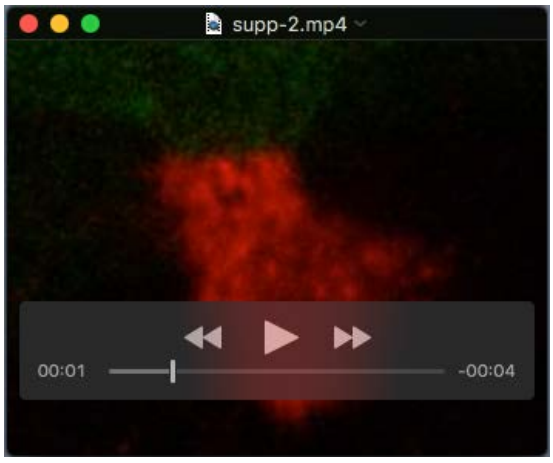

Movie S2: Spdo localization in *strat* SOP daughter cells

Localization of Spdo in *strat* SOP daughter cells from the apical pole to the basal pole (anti-Spdo, red).